

1 Astronomical calibration of upper Campanian–Maastrichtian carbon isotope events and
2 calcareous plankton biostratigraphy in the Indian Ocean (ODP Hole 762C): implication for
3 the age of the Campanian–Maastrichtian boundary

4

5 Nicolas Thibault^{a*}, Dorothée Husson^b, Rikke Harlou^a, Silvia Gardin^c, Bruno Galbrun^b, Emilia
6 Huret^d, Fabrice Minoletti^b

7

8 ^a Department of Geography and Geology, University of Copenhagen, Øster Voldgade 10,
9 1350 Copenhagen C., Denmark.

10 ^b Institut des Sciences de la Terre de Paris, UMR CNRS 7193, Université Pierre et Marie
11 Curie Paris 06, 4, place Jussieu, 75252 Paris cedex 05, France.

12 ^c « Paléobiodiversité et Paléoenvironnements », UMR CNRS 5143, Université Pierre et Marie
13 Curie Paris 06, 4, place Jussieu, 75252 Paris cedex 05, France.

14 ^d Andra, 1/7, rue Jean-Monnet, Parc de la Croix Blanche, 92298 Chatenay-Malabry cedex,
15 France.

16

17 * corresponding author, present address, nt@geo.ku.dk

18

19 **Abstract**

20

21 An integrated framework of magnetostratigraphy, calcareous microfossil bio-events,
22 cyclostratigraphy and $\delta^{13}\text{C}$ stratigraphy is established for the upper Campanian–Maastrichtian
23 of ODP Hole 762C (Exmouth Plateau, Northwestern Australian margin). Bulk-carbonate $\delta^{13}\text{C}$
24 events and nannofossil bio-events have been recorded and plotted against
25 magnetostratigraphy, and provided absolute ages using the results of the cyclostratigraphic
26 study and the recent astronomical calibration of the Maastrichtian. Thirteen carbon-isotope
27 events and 40 nannofossil bio-events are recognized and calibrated with cyclostratigraphy, as
28 well as 14 previously published foraminifer events, thus constituting a solid basis for large-
29 scale correlations. Results show that this site is characterized by a nearly continuous
30 sedimentation from the upper Campanian to the K-Pg boundary, except for a 500 kyr gap in
31 magnetochron C31n. Correlation of the age-calibrated $\delta^{13}\text{C}$ profile of ODP Hole 762C to the
32 $\delta^{13}\text{C}$ profile of the Tercis les Bains section, Global Stratotype Section and Point of the
33 Campanian–Maastrichtian boundary (CMB), allowed a precise recognition and dating of this
34 stage boundary at 72.15 ± 0.05 Ma. This accounts for a total duration of 6.15 ± 0.05 Ma for the
35 Maastrichtian stage. Correlation of the boundary level with northwest Germany shows that
36 the CMB as defined at the GSSP is ~ 800 kyr younger than the CMB as defined by Belemnite
37 zonation in the Boreal realm. ODP Hole 762C is the first section to bear at the same time an
38 excellent recovery of sediments throughout the upper Campanian–Maastrichtian, a precise
39 and well-defined magnetostratigraphy, a high-resolution record of carbon isotope events and
40 calcareous plankton biostratigraphy, and a cyclostratigraphic study tied to the La2010a
41 astronomical solution. This section is thus proposed as an excellent reference for the upper
42 Campanian–Maastrichtian in the Indian Ocean.

43

44 Keywords: Late Cretaceous; calcareous nannofossils; planktic foraminifera; biostratigraphy;
45 $\delta^{13}\text{C}$ stratigraphy, cyclostratigraphy
46
47

48 **1. Introduction**

49

50 The Maastrichtian stage has been intensively studied the past 15 years after the
51 identification of several distinct climatic episodes (Barrera and Savin, 1999; Li and Keller,
52 1999) that impacted several biotic groups in the marine realm : Inoceramid bivalves
53 (MacLeod et al., 1996), rudist bivalves (Johnson et al., 1996), planktic foraminifera (Li and
54 Keller, 1998a, 1998b; Olsson et al., 2001; Abramovich and Keller, 2002, 2003) and
55 calcareous nannofossils (Friedrich et al., 2005, Thibault and Gardin, 2006, 2007, 2010). In the
56 pelagic realm, the correlation of these climatic episodes and associated biotic events mainly
57 relies on the confidence in planktic foraminifera and calcareous nannofossil biozonations,
58 along with magnetostratigraphy. Because polarity reversals are geologically rapid events that
59 are potentially recorded simultaneously in rocks all over the world, the use of
60 magnetostratigraphic divisions is the most reliable correlation tool, contrary to
61 lithostratigraphic and biostratigraphic divisions which are often time-transgressive. In Late
62 Cretaceous carbonates, magnetic properties are poorly recorded and good
63 magnetostratigraphic records along with calcareous microfossil events are only available for a
64 limited number of sections (Bralower et al., 1995 and references therein).

65 The climatic evolution of the latest Cretaceous is characterised by a long-term global
66 cooling trend that started in the late Campanian and led to increased bioprovinciality of
67 calcareous microfossil assemblages into distinct Tethyan, Intermediate (Transitional is rather
68 adopted here), Boreal and Austral Provinces that persisted to the end of the Maastrichtian
69 (Shafik, 1990; Huber, 1992a; Huber and Watkins, 1992; Burnett, 1998; Lees, 2002). This
70 seriously complicates the application of available biostratigraphical zonation schemes. Two
71 distinct Late Cretaceous Austral and Tethyan biozonal schemes exist for Planktic
72 foraminiferal assemblages (Premoli-Silva and Sliter, 1994; Huber, 1992b) whereas 3 distinct

73 biozonal schemes (TP for Intermediate and Tethyan provinces, BP for the Boreal Province
74 and AP for the Austral Province) were proposed by Burnett (1998) for Late Cretaceous
75 calcareous nannofossils. The BP and TP schemes have different nannofossil subzones but
76 similar zones.

77 Throughout the Campanian-Maastrichtian interval, Northwestern Australia was part of
78 the Transitional Province (Huber, 1992a, Huber and Watkins, 1992). Microfossil assemblages
79 from this region show affinities to the warm Tethyan Province and to the cool Austral
80 Province (Shafik, 1990; Howe et al., 2003, Campbell et al., 2004). Several authors noted the
81 difficulties in applying standard planktic foraminiferal and nannofossil Tethyan
82 biostratigraphical zonal schemes to the Campanian-Maastrichtian interval of northwestern
83 Australia due to the absence of key markers or to variations in the ranges of these species
84 (Apthorpe, 1979; Wonders, 1992; Bralower and Siesser, 1992; Shafik, 1998; Petrizzo, 2000;
85 Howe et al, 2003). Petroleum companies that operate in northwestern Australia use the
86 regional KCCM (Cretaceous Composite Calcareous Microfossil) zonation which integrates
87 nannofossil, planktonic foraminiferal and benthic foraminiferal bio-events. This zonation was
88 successfully applied to numerous sites of Western Australian Phanerozoic basins (Howe et al.,
89 2003; Campbell et al., 2004). The example of the North Australian margin shows that
90 possible diachronism of key calcareous microfossil bio-events across latitudes needs to be
91 properly tested and eventually quantified in order to improve the correlation between AP, TP
92 and BP schemes.

93 In addition, high-resolution bulk carbonate $\delta^{13}\text{C}$ reference curves have started to be
94 generated for the Maastrichtian stage (Voigt et al., 2010; Thibault et al., 2012, Voigt et al.,
95 2012) but have not been tied to cyclostratigraphy so far. Because $\delta^{13}\text{C}$ is not dependent to
96 temperature and more robust than $\delta^{18}\text{O}$ to diagenesis, the use of carbon stable-isotope profiles
97 calibrated with detailed biostratigraphies have proved to be a powerful tool for correlating and

98 dating Cretaceous strata on a global scale (Gale et al., 1993; Jenkyns et al., 1994; Voigt, 2000;
99 Jarvis et al., 2002; Föllmi et al., 2006).

100 This paper presents new results on calcareous nannofossil biostratigraphy, carbon
101 stable isotopes and cyclostratigraphy throughout the upper Campanian–Maastrichtian section
102 of Hole 762C (Northwestern Australian margin) for which magnetostratigraphy was well
103 established (Galbrun, 1992) and recently updated (Husson et al., 2011, 2012). Using the
104 results obtained with the cyclostratigraphic study and the recent astronomical calibration of
105 the Maastrichtian (Husson et al., 2011), we calibrate all carbon isotopic and biotic events in
106 age and propose a new chronostratigraphic reference for the Indian Ocean. The calibrated
107 chronostratigraphic framework is then correlated and compared to reference sites in the
108 Tethyan and Boreal realms and allows a focus on the correlation and age of the Campanian–
109 Maastrichtian boundary at the global scale.

110

111 **2. Exmouth Plateau : setting and previous work**

112

113 ODP Hole 762C (19°53.24'S, 112°15.24'E) was drilled at a water depth of 1360 m in
114 the western part of the central Exmouth Plateau, off NW Australia in the eastern Indian Ocean
115 (Fig. 1). Sediments were deposited in an upper bathyal setting (Zepeda, 1998). The estimated
116 palaeolatitude of this site is 43°S using Ocean Drilling Stratigraphic Network (ODSN) plate
117 tectonics reconstruction (Based on Hay et al., 1999). The studied interval almost spans the
118 whole Maastrichtian stage from the K-Pg boundary to magnetochron C33n downhole (Fig. 2).
119 This interval recovers Subunit IVA and the upper part of Subunit IVB which correspond to
120 nannofossil chalks with varying amounts of clays and foraminifers (Haq et al., 1992).
121 Sediments consist of white to very light green-gray nannofossil chalk (light beds) alternating
122 with intervals of light green-gray clayey nannofossil chalk (dark beds). These cyclic color

123 changes of light and dark beds without distinct limits reflect the relative abundance of clay
124 and calcium carbonate (Haq et al., 1992). These cycles were deposited under a Milankovitch
125 control (Golovchenko et al., 1992; Huang et al., 1992). The biostratigraphy of planktonic
126 foraminifera was first established by Wonders (1992) and revised by Zepeda (1998). The
127 biostratigraphy of calcareous nannofossils was established by Bralower & Siesser (1992) and
128 refined in this study with a higher resolution. Howe et al. (2003) and Campbell et al. (2004)
129 provided a detailed regional, composite biostratigraphic zonation of this site using numerous
130 calcareous nannofossil, planktic and benthic foraminiferal bio-events. The
131 magnetostratigraphy was first established by Galbrun (1992) and refined in Husson et al.
132 (2011, 2012). All the magnetostratigraphic signals of the standard magnetic polarity time scale (Gradstein
133 et al., 2004) have been retrieved with a high precision and very few uncertainties across
134 boundary reversals (Appendix 1). Hole 762C bears one of the best defined
135 magnetostratigraphic signals throughout the upper Campanian–Maastrichtian along with Site
136 525A in the South Atlantic (Chave, 1984) and the Bottaccione and Contessa sections in
137 central Italy (Gardin et al., 2012). The lower half of the astronomical calibration of the
138 Maastrichtian also relies on this site (Husson et al., 2011) and the detailed cyclostratigraphic
139 analysis of this section is presented here. ODP Hole 762C thus constitutes the only section
140 that bears at the same time (1) an excellent recovery of sediments throughout the upper
141 Campanian–Maastrichtian, (2) a very precise and well-defined magnetostratigraphy with all
142 magnetostratigraphic signals and subchrons of this period identified, (3) a record of calcareous nannofossil
143 and planktonic foraminifera bio-events and (4) a high potential for a cyclostratigraphic study
144 tied to the recent astronomical calibration of the Maastrichtian.

145

146 *Figure 1 about here: format one column, 8 cm wide*

147 *Figure 2 about here: format landscape on full page*

148

149 **3. Materials and methods**

150

151 *3.1. Micropaleontological analysis*

152

153 167 samples of ODP Hole 762C were processed as follows : sediments were gently
154 disaggregated in a mortar and 50 mg of dried sediment were weighed and dispersed in 50 ml
155 of distilled water. The suspension was ultrasonicated for 15 sec and homogenized with a
156 magnetic stirrer. Then 1mL of this suspension was extracted with a finnpipette and
157 homogeneously dropped on a microscopic slide. Particles are therefore evenly distributed on
158 the slide.

159 Semi-quantitative counts were performed on key and other potential additional
160 stratigraphic markers (Appendix 2) at a magnification of x1600 (x100 oil objective with a
161 x1.6 additional lense). Counts were determined in the following fashion: a species was
162 determined as abundant (A) if, on average, more than 10 specimens could be observed in a
163 field of view; common (C) if one to 10 specimens could be observed in each field; few (F) if
164 one specimen or more could be observed in every 10 fields of view, rare (R) if, on average,
165 only one specimen could be observed in 11 to 100 fields, single (S) if only one specimen was
166 observed during the investigation. Preservation of nannofossils ranges from moderate (M) to
167 poor (P) in the investigated section.

168 The biozonation of Burnett (1998) was applied. Calcareous nannofossil species
169 considered in this paper followed taxonomic concepts of Perch-Nielsen (1985) and Young &
170 Bown (1997). Bibliographic references for the determined taxa are given in Perch-Nielsen
171 (1985), Bown (1998) and Howe et al. (2003).

172

173 3.2. *Cyclostratigraphic analysis*

174

175 As many of Deep Sea Drilling Project (DSDP) and ancient Ocean Drilling Program
176 (ODP) sections, Hole 762C lacks high-resolution geophysical measurements that could be
177 used for a cyclostratigraphic analysis. However, it has been shown that high-resolution core
178 photographs can be used for such a purpose (Cramer, 2001). A Gray-scale log was generated
179 on core photographs from the upper Campanian–Maastrichtian interval of this hole, available
180 on the ODP website (http://www-odp.tamu.edu/publications/122_IR/122TOC.HTM). Each
181 photograph displays one ODP core, with sections of the core arranged parallel to one another
182 (Fig. 3). For each section, gray-scales logs were processed using the free open-source
183 software Image-J (<http://rsb.info.nih.gov/ij/>) with a scaling of 2100 pixels for each 1.5 m long
184 section (Fig. 3). Gray-scale logs reflect the values of pixels along a line traced in the centre of
185 each section with a corresponding sampling interval of about 0.7 mm. Gray-scale values were
186 then smoothed and resampled at 1 cm intervals (Appendix 4).

187 Contrary to Cramer (2001) who adjusted core depths by removing all voids and
188 contracting cores for which the measured length was longer than the drilled length, we chose
189 to consider intervals of no recovery which can either represent a void or loss of recovered
190 material, and to keep additional lengths, in order not to potentially contract sedimentary
191 cycles. Adjusted depths were generated and are given in ‘ambsf’ units.

192 Fractures present on the core photographs, characterized by very low gray-level
193 values, close to 0, were removed from the original signal using a MATLAB script as
194 explained in Husson et al. (2011).

195 The effects of lighting on the photographs were treated by the recognition and filtering
196 of cycles with a period of 1.5 m (length of a section), 6.5 and 8.5 to 9.5 m (lengths of distinct
197 cores).

198 The resulting data were then analyzed via spectral analysis using the multitaper
199 method (MTM, Thomson, 1982). More detailed methodology for the cyclostratigraphic
200 analysis is given in Husson et al. (2011).

201

202 *Figure 3 about here: format one column, 8 cm wide*

203

204 3.3. Stable isotope analysis

205

206 A total of 200 stable isotope analyses has been performed throughout the late
207 Campanian–Maastrichtian of ODP Hole 762C. Oxygen and carbon isotopic composition of
208 bulk carbonates were measured with a mass spectrometer Finnigan Delta E on 87 samples at
209 the Laboratoire Biominéralisations et Paléoenvironnements (Université Pierre et Marie Curie,
210 Paris 6, France) in 2007. The extraction of CO₂ was done by reaction with anhydrous
211 orthophosphoric acid at 50°C. Additional analyses were performed with a micromass
212 isoprime spectrometer on 113 bulk carbonates at the Department of Geography and Geology,
213 University of Copenhagen in 2009. The extraction of CO₂ was done by reaction with
214 anhydrous orthophosphoric acid at 70°C. The oxygen and carbon isotope values are expressed
215 in per mil relative to the V-PDB standard reference. The analytical precision is estimated at
216 0.1‰ for oxygen and 0.05‰ for carbon for both laboratories. Common samples and samples
217 from the same stratigraphic intervals show a constant offset of -0.25‰ for δ¹⁸O values and -
218 0.2‰ for δ¹³C values between measurements from 2009 and those from 2007, likely due to
219 the different methods and apparatus. Values of 2007 were thus adequately corrected for
220 standardization. Inter-laboratory offsets of 0.1 to 0.2 per mil can commonly occur when
221 laboratories use single-point anchoring with one certified internal standard. Inter-laboratory

222 normalization producing minimal errors <0.1 per mil is possible only when laboratories use
223 anchoring with two or more certified internal standards (Debajyoti et al., 2007).

224

225 **4. Results**

226

227 *4.1. Calcareous microfossil biochronology*

228

229 Foraminifera bio-events recorded in Howe et al. (2003) and Campbell et al. (2004) are
230 reported here along with magnetostratigraphy, carbon-isotope stratigraphy and nannofossil
231 biostratigraphy refined in this study (Fig. 2). The resolution of the nannofossil analysis is ca. 1
232 m across the studied interval and below 0.5 m in the interval between 620 and 595 mbsf
233 where a large number of bio-events were recorded (Fig. 2). In addition to the record of typical
234 first (FO) and last occurrences (LO) of taxa, few particular features are proposed here as bio-
235 events. A transition in the abundance of *Watznaueria manivitae* sensu lato was observed with
236 abundances shifting from common to frequent at 649.63 mbsf (Chron C33n, upper
237 Campanian) (Fig. 2). As in Lees and Bown (2005), two different forms of *Uniplanarius*
238 *trifidus* with distinct stratigraphic levels of extinction were observed, a medium-rayed and a
239 short-rayed form (Fig. 2). Three species also exhibit intervals of acmes: *Cribracorona gallica*
240 (561.4 to 559.08 mbsf), *Micula murus* (564.14 to 556.33 mbsf) and *Lithraphidites* spp. (573.6
241 to 561.4 mbsf) (Fig. 2). This provides a total record of 18 foraminifer bio-events, 40
242 nannofossil bio-events and 4 additional nannofossil events based on obvious changes of
243 abundances correlated to carbon-isotope stratigraphy (Fig. 2 and Table 1).

244

245 *Table 1 about here: format portrait*

246

247 *4.2. Cyclostratigraphy*

248

249 *4.2.1. Spectral analysis and amplitude spectrogram*

250

251 The respective thickness of magnetochrons C31r and C30n relative to their duration,
252 according to the Geologic Time Scale 2004 (GTS2004, Gradstein et al., 2004), suggest
253 variations of the sedimentation rate. To ascertain these variations, spectral analyses have been
254 performed on two different intervals: the upper Campanian–lower Maastrichtian interval,
255 from 593 to 638 ambsf, and the upper Maastrichtian from 550 to 593 ambsf. The study of the
256 lower Maastrichtian periodogram highlights cycles with wavelength ranging from 0.26 to 4.1
257 m, with low frequency cycles presenting the highest power and the best individualisation
258 (Fig. 4). Comparison of their period ratios with the ratio of orbital parameters periods has
259 permitted their attribution to a forcing by the 405 kyr eccentricity (2.15 to 4.1 m cycles), 100
260 kyr eccentricity (0.58 m to 0.75 m cycles), and obliquity (0.26 m) variations (Fig. 4). The
261 identification of groups of cycles rather than distinct periods is linked to sedimentation rate
262 variation within the studied interval, which modifies the thickness of the cycles (Herbert,
263 1994).

264 The spectral analysis performed between 550 and 593 ambsf (upper Maastrichtian)
265 detects cycles with a wavelength ranging from 0.40 to 7.46 m (Fig. 4). The periodogram
266 shows numerous low frequency cycles and less expressed high frequencies variations. The
267 frequency ratios method applied to the periodogram indicates a forcing of the sedimentation
268 by obliquity, 100 kyr eccentricity, and 405 kyr eccentricity (Fig. 4). Colour variations in the
269 upper Maastrichtian have less amplitude, and the power of 405 kyr cycles is attenuated in the
270 frequency spectrum of the 550-593 ambsf interval as compared to the interval below (Fig. 4).
271 This strong attenuation and a disturbance due to the presence of numerous cracks in the

272 “strange” interval between 576 and 588 ambsf hindered the recognition of clear 405 kyr
273 cycles in the amplitude spectrograms of the upper Maastrichtian (Fig. 4). In addition, apart
274 from one interval in core 48X between 604 and 610 ambsf (Figs. 3–4), precession cycles are
275 not very well defined on the periodograms and in amplitude spectrograms. The studied
276 intervals may be too large to highlight high frequency cycles with accuracy. A strong shift of
277 the cycles toward lower frequencies can be observed between the two periodograms. It
278 characterises an increase of the sedimentation rate in the upper Maastrichtian.

279

280 *Figure 4 about here: format portrait full page*

281

282 Amplitude spectrograms characterize shifts in the frequency of Milankovith cycles and
283 variations of the sedimentation rate. Well-defined trends present on the entire record are
284 related to the evolution of 100 kyr and 405 kyr eccentricity cycles by comparison to the
285 results of the spectral analysis (Fig. 4). Obliquity is well characterised in the upper
286 Campanian and is also recorded during the lower Maastrichtian, though its amplitude is lower
287 (Fig. 4). Eccentricity is disturbed between 612.5 and 607.5, due once again to important core
288 cracks in this interval (Fig. 4). This interval also corresponds to decreasing sedimentation
289 rates. Sedimentation rates are much higher in the upper Maastrichtian as suggested by the
290 shift of 100 kyr eccentricity cycles toward lower frequencies after the “strange” disturbed
291 interval (Fig. 4). Perturbations of the analysis in the higher frequencies, due to the remaining
292 cracks in the cores, prevent a good identification of precession and obliquity variations. For
293 the upper Maastrichtian, only a filtering of 100 kyr eccentricity cycles could be performed
294 because doubts remained on the identification of 405 kyr cycles attenuated in the frequency
295 spectrum and hindered in the amplitude spectrograms. For the upper Campanian and lower
296 Maastrichtian, a filter output of the 405 kyr eccentricity was performed from the lowermost

297 part of Chron C31n down to the upper part of Chron C33n. This filter output was already
298 presented in Husson et al. (2011) and calibrated to the La2010a astronomical solution (Laskar
299 et al., 2011).

300 The identification of 100 kyr and 405 kyr eccentricity cycles allows estimation of durations
301 by cycle counting. The counting is performed considering that minima in grey values (darker
302 colours) might correspond to maxima of insolation. Indeed, darker sediments have higher
303 terrigenous content which seem to reliably reflect enhanced weathering during periods of
304 higher insolation throughout the Cenozoic and Cretaceous period (Pälike et al., 2006,
305 Westerhold et al., 2008, Batenburg et al., 2012).

306 When precession cycles are well defined, the resolution in the cycle counting can be
307 down to 20 kyr (Fig. 3). Cycle counting was performed on a 5 points moving average
308 smoothed grey scale signal and relies on the 100 kyr filter output (Fig. 5). 100 kyr and 405
309 kyr eccentricity cycles have been numbered downhole with the Cretaceous/Paleogene (K-Pg)
310 boundary as starting point. Filtering can induce phase-shifts and create a misleading
311 impression of regular cyclicity where grey level variations are important (Weedon, 2003).
312 This effect has been limited by using a very large bandwidth.

313

314 *Figure 5 about here: Format portrait full page*

315

316 4.2.2. *Downhole 100 kyr numbering and age-calibration of calcareous plankton bio-events*

317

318 The position of the boundary between chrons C30n and C29r has been revised here
319 and is given a much larger uncertainty than in Galbrun (1992). Indeed, most of the samples of
320 core 43X2 to core 43X5 analysed by Galbrun (1992) could not be demagnetized at high steps,
321 given their weakness in NRM intensity. As a consequence, these samples showed a weak

322 negative inclination which was previously interpreted as a normal polarity (Galbrun, 1992).
323 However the sub-jacent well-magnetized sample 44X1-132 (565.32 mbsf), shows a strong
324 positive inclination, interpreted as a short interval of reversed polarity (Galbrun, 1992) and is
325 then followed by numerous well-magnetized samples of normal polarity. Thus, the base of
326 C29r which was previously placed at 556.5 mbsf could also be placed downhole at 565.32
327 mbsf. Moreover, according to Henriksson (1993) whose study focused on the biochronology
328 of *Micula prinsii* biozone on a large number of sites, the FO of this taxon is synchronous
329 throughout the tethyan and transitional realms and lies very close to the base of magnetochron
330 C29r. In our study, the FO of this taxon is recorded at 560.46 mbsf (Fig. 2 and Table 1). A
331 downhole position of the base of C29r may thus be expected. The interval of no recovery at
332 the base of core 43X further complicates the precise identification of the boundary between
333 C29r and C30n. As a consequence, the whole uncertainty (between 556.5 and 565.32 mbsf) is
334 taken into account and the C29r/C30n boundary is rather placed at 560.91 +/- 4.41 mbsf
335 (Table 2a, Fig. 2). This new position results in a duration of 397 +/- 221 kyr for the
336 Cretaceous part of C29r which is consistent with the estimation provided in Husson et al.
337 (2011). However, the latter provided a much more precise and reliable estimation of the
338 duration of the Cretaceous part of chron C29r which is rather adopted here.

339 The duration and ages of biostratigraphic events and carbon-isotope trends rely
340 precisely on the downhole numbering of 100 kyr cycles (Fig. 5). This numbering is based on
341 the cycles identified according to the results of spectral analyses and can be followed on
342 Figure 5 along the 100 kyr filter output. The numbering also remains in accordance with the
343 astronomical calibration of the Maastrichtian tied to the La2010a astronomical solution
344 (Husson et al., 2011). The following reasoning has been followed for the different gaps of the
345 record: (1) Consistency in the thickness of the cycles has been assumed for all the intervals of
346 no recovery, except for the interval centered around 592 mbsf (Fig. 5). (2) Cyclostratigraphic

347 interpretations at Sites 1267B and 525A showed that chron C30r partly covers 100 kyr
348 eccentricity cycles e_{10023} and e_{10024} (Husson et al., 2011, Figure 3). Two samples clearly
349 indicated a reverse polarity around 595 ambsf (Appendix 1) and a total uncertainty of 4.3 m is
350 accounted for the boundary between chrons C30n and C30r (Fig. 2 and Table 2a). Therefore,
351 we have assigned the interval of no recovery between 591 and 594 ambsf as well as a short
352 part of the filter output between 594 and 594.6 ambsf to e_{10023} and the following cycle to
353 e_{10024} , ending around 596.5 ambsf (Fig. 5). (3) A maximum of four 100 kyr eccentricity
354 cycles can be identified in the interval between 596.5 and 599.5 ambsf corresponding to
355 Chron C31n (Fig. 5). This contrasts with Herbert et al. (1999) and Husson et al. (2011) who
356 showed an average duration of this chron of 900 kyr. Therefore, a gap of ca. 500 kyr can be
357 accounted here and likely placed around 597 ambsf, where a neat change in the sedimentation
358 rate can be observed while comparing the thickness of e_{10023} and e_{10024} with the underlying
359 cycles (Fig. 5). This gap corresponds to the darkest interval of core 47X which could suggest
360 a much lower carbonate input to the sea-floor responsible for very low sedimentation rates.
361 Downhole numbering of the following cycles takes into account this 500 kyr gap and further
362 remains consistent with the numbering of 100 kyr eccentricity cycles at Sites 525A and
363 1258A with an average assignment to the base of e_{10033} for the base of Chron C31n (Fig. 5,
364 Husson et al., 2011, Figure 3) and with the calibration of these three sites to the La2010a
365 astronomical solution (Husson et al., 2011, Figure 5). Uncertainties are low for the boundaries
366 of the following magnetostratigraphic units of the lower Maastrichtian and upper Campanian (Tables 2a
367 and 2b).

368 Foraminifera and calcareous nannofossil bio-events recorded in Hole 762C are
369 calibrated in ages using the results of the cyclostratigraphic study (Table 1). Age uncertainties
370 on the ages of bio-events are calculated by taking into account the uncertainty between top
371 and bottom depths as well as the uncertainty on the ages of the K/Pg boundary (0.07 Ma,

372 Husson et al., 2011). An age of 66 Ma for the K-Pg was chosen based on the recent results on
373 radiometric dating and astronomical calibrations of the Paleocene (Kuiper et al., 2008;
374 Westerhold et al., 2008; Hilgen et al., 2010; Renne et al., 2010). This provides a robust
375 stratigraphic framework that can be used as a reference for the Indian Ocean and also provides
376 a base for large-scale correlations and testing in the future of potential
377 synchronism/diachronism of planktonic microfossil bio-events between the different
378 provinces of the southern hemisphere.

379

380 *Table 2a and 2b about here*

381

382 *4.3. Carbon stable isotopes*

383

384 A cross-plot of carbon- and oxygen-isotope values (Fig. 6) shows no significant trends
385 and lacks the pronounced covariance seen in many mixing lines produced by the addition of
386 variable quantities of isotopically homogeneous diagenetic cement to isotopically
387 homogeneous skeletal calcite (Jenkyns et al., 1995; Mitchell et al., 1997). The pattern of $\delta^{13}\text{C}$
388 values generally conforms to trends observed in bulk stable isotopes of a number of reference
389 sites (Figs. 7–10). Given that chalk sediments of Hole 762C are mainly composed of
390 calcareous nannofossils, the characteristic form of this curve likely reflects primary sea-
391 surface water values with minimal diagenetic effects affecting the section in generally
392 consistent manner.

393 Due to the higher ratio of oxygen in interstitial fluids with respect to oxygen in
394 carbonate as compared to similar ratio of carbon, and due to their thermo-dependence, oxygen
395 isotopes are far more sensitive to post-depositional processes which increase with the porosity
396 of the sediment (Schrag et al., 1995). In chalks of ODP Hole 762C, oxygen isotope values are

397 highly variable which may reflect the Milankovitch control on the sedimentation enhanced by
398 diagenesis. No clear long-term trends or trends conformed to previously published planktic
399 foraminifera $\delta^{18}\text{O}$ profiles worldwide (Barrera and Savin, 1999) were observed in our
400 analysis. Diagenetic overprint may have altered primary $\delta^{18}\text{O}$ values which are thus not
401 presented here.

402 Carbon isotope values range between 2.35 and 3.1‰ and do not display any
403 significant difference with respect to colour alternations (Fig. 2). The carbon isotope profile
404 exhibits several positive and negative excursions and inflection points which are calibrated in
405 age using the cyclostratigraphic results from the K-Pg boundary to 645 ambsf (642.65 mbsf)
406 downhole. The rest of the profile was calibrated in age considering an average sedimentation
407 rate of 14.5 m/Ma similar to the interval above between 634 and 644 ambsf (Figs. 7–11).

408 Despite some local expressions probably due to changing sedimentation rates and
409 occurrence of stratigraphical gaps, the patterns of $\delta^{13}\text{C}$ values found at Site 762C well
410 conforms to trends observed in bulk stable isotopes of a number of sites of the same age. The
411 pattern of $\delta^{13}\text{C}$ values conforms to trends observed in bulk stable isotopes of Tercis les Bains
412 (Fig. 7), of the Gubbio composite curve (Fig. 7), of the Lägerdorf – Kronsmoor – Hemmoor
413 (LKH) section in Northwest Germany (Fig. 8), in stable isotopes of planktic and benthic
414 foraminifera in South Atlantic DSDP Hole 525A (Fig. 9) and in the Indian Ocean ODP Hole
415 761 (Barrera and Savin, 1999). The most prominent $\delta^{13}\text{C}$ events identified in common in the
416 nearby Indian Ocean Site 761 and in other reference sites fall within the same magnetochrons
417 and, approximately, within the same subparts of magnetochrons, thus making a high degree of
418 reliability (Figs. 7–9).

419 *Figure 6 about here: format one column, ~ 8 cm wide*

420

421 These correlations helped to define 13 isotopic events in ODP Hole 762C whose
422 description is given below (Figs. 7–10 and Table 3).

423 A short negative excursion (C1-) is identified in the uppermost Campanian right at the
424 base of chron C32n2n above the LO of *Eiffelithus eximius* (Fig. 2). This excursion is
425 characterized by a sharp 0.25‰ negative shift, a small rebound and another 0.1‰ negative
426 shift (Figs. 7–8). This event is poorly defined in Hole 762C, where values do not come back
427 to pre-excursion levels at the top of the event as observed in Tercis les Bains, LKH or Gubbio
428 (Figs. 7–8). C1- event, also identified at the base of C32n2n at Gubbio (Fig. 7) has an
429 estimated duration of ~300 kyr in Hole 762C (Table 4), which matches the 405 kyr filtering in
430 LKH (Fig. 8).

431 The three-step negative shift of the Campanian – Maastrichtian boundary defined as
432 CMB a, CMB b and CMB c (Thibault et al., 2012) is identified within chron C32n2n in Hole
433 762C, in accordance with the results of Tercis les Bains and Gubbio (Fig. 7). The LOs of
434 *Uniplanarius trifidus* and *U. gothicus* are recorded within CMB c in Hole 762C and above
435 this event at Tercis les Bains (Fig. 7). In addition, the LO of *T. stemmerikii* is recorded within
436 CMB c both in Hole 762C and in Stevns-1 (Fig. 8).

437 Nearly all Maastrichtian $\delta^{13}\text{C}$ events defined in Stevns-1 (Thibault et al., 2012) can be
438 identified in Hole 762C and in the LKH section, resulting in a precise correlation between the
439 three sections (Fig. 8). One exception concerns the identification of M3-(b), a small and short-
440 lived negative excursion in Stevns-1 and LKH and well-defined event named MME for Mid-
441 Maastrichtian event in the Gubbio curve (Fig. 7, Voigt et al., 2012). This event falls into the
442 identified gap in Hole 762C (Figs. 7–8).

443 A 0.4‰ positive excursion between M3-(b) and M4-(a) occurs in the lower half of
444 chron C30n in Hole 762C (Fig. 7). This excursion is also observed in the same chron at ODP
445 Hole 761, another site of the Exmouth Plateau in the Indian Ocean (Barrera and Savin, 1999,

446 Fig. 6B) as well as at Site 1210B in the Pacific Ocean (Voigt et al., 2012). This positive
447 excursion, not observed in Stevns-1, is more evident in LKH and better expressed at Gubbio
448 composite curve (Figs. 8–9). However, the fairly large extent of this event, that we named as
449 Exmouth Plateau event (Figs. 7–10), rather points to a regional peculiarity (+0.4‰ in Hole
450 762C versus 0.1‰ at Gubbio) (Fig. 7) .

451

452 *Figure 7 about here: format portrait full page width*

453 *Figure 8 about here: format landscape on full page*

454 *Figure 9 about here: format landscape on full page*

455 *Table 3 about here: format portrait full page width*

456 *Table 4 about here*

457

458 **5. Discussion**

459

460 *5.1. Early Maastrichtian disconformity or diachronism of microfossil bio-events ?*

461

462 Howe et al. (2003) identified an early Maastrichtian disconformity in sites from the
463 Exmouth Plateau (Hole 762C and 761B) within biozones KPF3/KPF2c (nannofossil zone
464 UC18, Fig. 2) based on the stratigraphic order of nannofossil and foraminifera bio-events
465 which differs from Tethyan stratigraphic frameworks. This assumption is mainly based on the
466 last co-occurrence of *Broinsonia parca constricta* and *Reinhardtites levis* and the very close
467 first occurrence of *Abathomphalus mayaroensis* (Fig. 2). Apthorpe (1979) previously
468 suggested that this early Maastrichtian disconformity is widespread on the western Australian
469 margin as she was unable to identify foraminifer biozone C12 in 45 of 52 wells from this area.
470 This disconformity would thus lie within chron C31r in Hole 762C (Fig. 2). No hiatus can be

471 characterized in the amplitude spectrograms of Hole 762C within chron C31r (Fig. 4).
472 Moreover, the obtained duration estimated in this section for chron C31r matches almost
473 perfectly those obtained at the Contessa highway section, central Italy (Husson et al., 2012),
474 as well as at Hole 1258A, Demerara Rise, central Atlantic (Husson et al., 2011). This result
475 differs from the duration provided in the GTS2004 by only 160 kyr (Table 2b). These results
476 do not suggest such a disconformity in Hole 762C. During the late Campanian and
477 Maastrichtian, the Perth and Carnarvon basins in the south of the western Australian margin
478 were shown to have Austral affinities whereas the northwestern margin where the Exmouth
479 Plateau is situated had Transitional affinities between Austral and Tethyan assemblages
480 (Rexilius, 1984; Shafik, 1990 ; Huber, 1992a; Huber and Watkins, 1992) (Fig. 1).
481 Diachronism of Late Cretaceous planktic foraminifer and nannofossil datums with respect to
482 paleolatitude in the Southern Ocean was discussed by Huber and Watkins (1992) and Petrizzo
483 (2003). Gardin et al. (2012) also discussed calcareous plankton diachronism and the difficult
484 applicability of the available “standard” calcareous nannofossil biozonations for the the late
485 Campanian–Maastrichtian. In the latest Cretaceous, during times of climatic cooling, standard
486 Tethyan zonations are difficult to apply because some index species are absent or have
487 different age ranges (Bralower and Siesser, 1992; Wonders, 1992; Petrizzo, 2000, 2003;
488 Howe et al., 2003; Campbell et al., 2004). Barrera and Savin (1999) and Li and Keller (1999)
489 showed that a global climatic cooling occurred right before the C32n/C31r transition and was
490 followed by warming in the topmost part of chron C31r. These climatic changes were mainly
491 deciphered through the oxygen isotope ratios of benthic foraminifera but also affected surface
492 waters as expressed by changes in calcareous nannofossil assemblages (Thibault and Gardin,
493 2006, 2007, Thibault et al., 2011). Therefore, the different order of nannofossil and
494 foraminifera bio-events observed in Hole 762C within chron C31r are rather the expression of

495 diachronism between Transitional and Tethyan provinces due to these climatic changes than
496 the evidence of a disconformity.

497

498 5.2. Age of the Campanian–Maastrichtian boundary

499

500 Before the ratification of the GSSP boundary at Tercis les Bains, the base of the
501 Maastrichtian stage was assigned to the first occurrence of belemnite *Belemnella lanceolata*
502 with reference to the chalk section of Krons Moor, North Germany (Birkelund et al., 1984;
503 Schönfeld et al., 1996). However, this marker has a biogeographic distribution which is
504 limited to the Boreal realm (Odin, 1996). The Maastrichtian Working Group chose to identify
505 the base of the Maastrichtian by the first occurrence of ammonoid *Pachydiscus neubergicus*
506 (Odin, 1996), which has a much wider geographical distribution (Hancock, 1991), on the
507 basis of indirect correlations and comparison of strontium isotope stratigraphy with the U.S.
508 Western Interior (McArthur et al., 1992; Landman and Waage, 1993; Schönfeld et al., 1996).
509 Subsequently, the Campanian–Maastrichtian GSSP boundary was defined and ratified at
510 Tercis les Bains close to the first occurrence of ammonoid *P. neubergicus* (the preferred guide
511 event, Odin and Lamaurelle, 2001) and as the arithmetical mean of 12 distinct biohorizons in
512 order to get the best precise definition. This combination of criteria ensures more secure
513 correlation of the boundary level at the global scale (Odin and Lamaurelle, 2001) than just the
514 ammonite bio-horizon only. Based on a large array of paleontological, paleomagnetic and
515 radiometric considerations, the GSSP boundary was considered nearly contemporaneous to
516 the FO of *B. lanceolata* in the Boreal realm (lan in LKH section, Fig. 8), lies close to the
517 middle or in the upper part of chron C32n2n, and was assigned an age of 72.0 +/- 0.5 Ma
518 (Barchi et al., 1997; Lewy and Odin, 2001; Odin and Lamaurelle, 2001). In the GTS2004, two
519 distinct ages are proposed. (1) A first approximate age of 70.6 Ma is based on the supposed

520 last occurrence of nannofossil *Uniplanarius trifidus* at the top of belemnite *Belemnella obtusa*
521 zone in northwest Germany, calibrated with the strontium isotope curve of McArthur et al.
522 (1994) at ca. 69.9 Ma. This estimate is ~0.75 Myr younger than the boundary level at Tercis
523 les Bains, by assuming a constant sedimentation rate on this section. However, *U. trifidus* is
524 actually inconsistent in Germany because this species is mainly restricted to low latitudes
525 (Schönfeld et al., 1996; Burnett, 1998) and the strontium isotope age calibration method has
526 an uncertainty comprised between 0.8 and 1.5 Ma (McArthur et al., 1994). (2) A second
527 estimate at 71.3 Ma is given, based on a strontium isotope age projection of the FO of
528 *B. lanceolata* (Schönfeld et al., 1996) on the curve of McArthur et al. (1994).

529 None of these two estimates actually match the biohorizon criteria provided for the
530 GSSP boundary and they do not take into account the large uncertainty of the strontium
531 isotope age calibration. In Husson et al. (2011), the LO of *U. trifidus* was considered to be ca.
532 0.75 Myr younger than the CMB at Tercis les Bains, assuming an obliquity-driven metric
533 rhythm of the sedimentation (40 kyr/m, Odin and Amorosi, 2001). The LO of *U. trifidus* is
534 identified with great precision in ODP Hole 762C (614.06 +/-0.06 mbsf), allowing a
535 cyclostratigraphic assignment to the top of Ca₄₀₅1 (616.09 ambsf, Fig. 5, Ma₄₀₅16 in Husson
536 et al., 2011). Consequently, the CMB was previously placed in the lowermost part of Ca₄₀₅2
537 (corresponding to Ma₄₀₅17 in Husson et al., 2011), within the middle of 100 kyr eccentricity
538 cycle e₁₀₀68. However, uncertainties remain for the position of the CMB because the LO of *U.*
539 *trifidus* at ODP Hole 762C falls within the interval of reduced sedimentation rates (Fig. 10)
540 and because a reasonable diachronism of this bio-event between the Tethyan and Transitional
541 Provinces can not be completely ruled out.

542 The correlation of $\delta^{13}\text{C}$ events CMBa, CMBb and CMBc between Stevns-1, Tercis les
543 Bains, LKH, Gubbio and Hole 762C (Figs. 7–9) calls for a revision of the placement and
544 subsequent age of the CMB. The boundary as defined in Tercis les Bains lies within CMBc

545 (Fig. 7), thus leading to a much more precise correlation of the boundary and a location at
546 615.4 mbsf (617.37 ambsf) in Hole 762C, i.e. within Ca₄₀₅1 and e₁₀₀₆₂, in the uppermost part
547 of chron C32n2n (Fig. 5). A precise age of 72.15±0.05 Ma can thus be proposed for the CMB,
548 considering an average age of 66 Ma for the K-Pg boundary (Kuiper et al., 2008; Westerhold
549 et al., 2008; Hilgen et al., 2010; Renne et al. 2010). An independent approach to estimate the
550 age of the CMB has been recently documented in Voigt et al. (2012) based on macrofossil
551 biostratigraphic correlations of Inoceramids between Tercis les Bains and the Western Interior
552 Basin. Revised ⁴⁰Ar/³⁹Ar ages of two bentonites, bracketing ammonite zones tied to
553 Inoceramid zonation across the Campanian–Maastrichtian boundary interval of the Western
554 Interior Basin, gives an age of 72.2±0.2 Ma for the CMB.

555 In addition, the correlation of Hole 762C, Stevns-1 and LKH sections shows that the
556 CMB falls exactly at the base of the *Belemnella obtusa* zone in northwest Germany (Fig. 8).
557 The base of the *B. lanceolata* zone in the Boreal realm corresponds to the base of δ¹³C event
558 CMBa and is approximately two 405 kyr cycles older than the identified level for the CMB
559 (Fig. 8). Consequently, the CMB as defined by the Belemnite zonation in the Boreal realm is
560 ~800 kyr older than the CMB as defined in the GSSP of Tercis les Bains. This duration is
561 slightly greater than the 500 kyr discrepancy already estimated by Niebuhr and Esser (2003).
562 Gradstein et al. (2004) already proposed a projection of the base of the Maastrichtian stage as
563 defined in Tercis les Bains approximately at the base of the *Belemnella obtusa* zone of
564 northwest Germany and consequently estimated a 700 kyr discrepancy between the GSSP and
565 the base of *B. lanceolata*.

566

567 5.3. Variations of the sedimentation rate

568

569 Variations of the sedimentation rate can be precisely estimated at the scale of 100 kyr
570 and 405 kyr eccentricity cycles (Fig. 10). The resulting curves agree with the trends
571 delineated on the amplitude spectrograms and show a drop of sedimentation rates from ~1.5
572 cm/kyr in C33n/C32r to very low values around 0.6 cm/kyr throughout the top of C32n2n to
573 C31n. The sedimentation rate suddenly increases to ~1.3 cm/kyr close to the transition
574 between chrons C31n and C30r, right after the identified 500 kyr gap. A second increase in
575 the middle part of chron C30n results in a average value of the sedimentation rate of 1.9
576 cm/kyr (Fig. 10).

577

578 *Figure 10 about here: format landscape full page*

579

580 An interesting issue is the comparison of the variations of the sedimentation rate with
581 $\delta^{13}\text{C}$ variations at Hole 762C and with the sea-level record (Fig. 10). Kominz et al. (2008)
582 recently provided an updated sea-level record for the last 108 Ma through the backstripping of
583 corehole data from the New Jersey and Delaware Coastal Plains. The temporal resolution of
584 the sea level curve is quite low for comparison at the scale of one single stage (+/-1Ma for the
585 Late Cretaceous) and still bears large uncertainties (Fig. 10). The three sea-levels curves of
586 Miller et al. (2005), Kominz et al. (2008) and Haq et al. (1987) are rather different for this
587 time interval (Fig. 10). Taking into account age uncertainties of these sea-level curves, a late
588 Campanian–early Maastrichtian 3rd order regression can be observed in the three records and
589 may correlate to the large interval of lower $\delta^{13}\text{C}$ values between events CMBa and M3+ (Fig.
590 10). This interval is also marked by low values of the sedimentation rate in Hole 762C (Fig.
591 10).

592 Several hypothesis may explain the variations of the sedimentation rate such as
593 variations in pelagic carbonate productivity, changes in accommodation by variations of

594 subsidence or detrital supply, dissolution at the sea-floor and winnowing. At Site 762C,
595 variations of the sedimentation rate may actually reflect a change in the strength and
596 chemistry of bottom currents along the northwestern Australian margin. The early
597 Maastrichtian 3rd order regression was correlated to an episode of accelerated cooling
598 associated to an inferred reversal of the thermohaline circulation (Barrera et al., 1997). The
599 coincidence between this 3rd order regression and this episode of accelerated cooling suggests
600 a glacio-eustatic mechanism (Miller et al., 1999). These authors argued for the development
601 of a moderate Antarctic ice-sheet at that time. Such a short early Maastrichtian ice-age would
602 have intensified high-latitude formation of cooler and oxygenated bottom-waters and
603 increased latitudinal temperature gradients (Barrera et al., 1997; Barrera and Savin, 1999).
604 The Southern and Indian Oceans were isolated by geographical barriers between Antarctica
605 and South America and in the central Atlantic, which inhibited the free circulation of
606 intermediate to deep-waters. As a result, bottom-waters generated around Antarctica would
607 have flowed north past the northwestern Australian margin into the Tethys Ocean (Howe et
608 al., 2003). These cooler and well-oxygenated bottom waters may have been slightly more
609 corrosive. Alternatively, stronger bottom currents could have resulted in displacing the
610 pelagic rain further north of the site of deposition of Site 762C at that time. These bottom
611 waters could also have resulted into higher winnowing of the sea-floor. No sign of erosion,
612 condensation or winnowing was noticed in the original description of cores 47X to 49X which
613 correspond to this interval of reduced sedimentation rates (Haq et al., 1990) but this
614 interpretation calls for a more detailed examination of these cores. Nethertheless, any of these
615 processes would have been associated to this paleoceanographic reorganization and may
616 account for lower sedimentation rates within this interval. At the early-late Maastrichtian
617 transition (topmost part of chron C31r), the geographical barrier formed by the Rio Grande
618 Rise and Walvis Ridge in the Atlantic Ocean was breached by sea-floor spreading on the

619 Mid-Atlantic Ridge, allowing free circulation of bottom-waters between the North Atlantic
620 and Indian Oceans (Frank and Arthur, 1999). Such a return of warmer, less corrosive and less
621 powerful bottom-waters might eventually explain the following increase of the sedimentation
622 rate in the remaining part of the Maastrichtian (Fig. 10).

623

624 *5.4. Correlations and paleoenvironmental interpretation of carbon-isotope signals*

625

626 Li and Keller (1998a, 1998b) and Barrera and Savin (1999) described carbon isotope
627 trends on separated planktic and benthic foraminifera from a large number of deep-sea sites in
628 the Atlantic, Pacific, Indian and Southern Oceans using time control on paleomagnetic
629 reversal stratigraphy and/or Sr isotopes calibrated on paleomagnetic reversal stratigraphy.
630 Their absolute ages were therefore based on Cande and Kent (1995) for magnetostratigraphy.
631 These ages have been revised in the GTS2004, in particular for the K-Pg boundary whose
632 calibration shifted from 65 to 65.5 Ma and recently to 66 Ma (Kuiper et al., 2008; Westerhold
633 et al., 2008; Renne et al. 2010). This led to discrepant late Maastrichtian ages of isotopic
634 events presented here and those described by previous authors. However, the bulk $\delta^{13}\text{C}$ profile
635 of the Maastrichtian of Hole 762C resembles previous $\delta^{13}\text{C}$ profiles acquired on separated
636 foraminifera (Li and Keller, 1998a, 1998b; Barrera and Savin, 1999), though several
637 additional events are recorded here, likely due to the higher-resolution dataset of our study or
638 to the localized expression of some events. As discussed above, correlation of major $\delta^{13}\text{C}$
639 events can be achieved throughout the Indian Ocean, the Tethys, the South Atlantic and the
640 Boreal realm (Figs. 7–9).

641 Changes in the $\delta^{13}\text{C}$ record of marine carbonates are generally interpreted as a reflect
642 of changes in the ratio of burial fluxes of isotopically light C of organic matter to C in the
643 carbonates (Scholle and Arthur, 1980; Arthur et al., 1988; Weissert, 1989; Weissert et al.,

644 1998). Additional factors that can influence this record are the addition into the marine realm
645 of various external carbon species, such as terrestrial (through weathering), platform-derived
646 C_{org} and dissolved inorganic carbon (platform drowning), atmospheric CO_2 , or methane-
647 derived carbon from the dissociation of clathrates (Cerlings et al., 1993; Dickens et al., 1995;
648 Hesselbo et al., 2000; Kump and Arthur, 1999; Immenhauser et al., 2003; Weissert and Erba,
649 2004; Swart and Eberli, 2005; Panchuk et al., 2005, 2006, Föllmi et al., 2006). However,
650 processes generally associated to large ($>1.5\%$) $\delta^{13}C$ excursions during oceanic anoxic events
651 (OAEs) in the Jurassic, early and mid-Cretaceous can hardly be applied to Campanian-
652 Maastrichtian records because no black shales were deposited on a large-scale during this
653 interval and because carbon-isotope excursions recorded here in bulk carbonates are either
654 much smaller ($\leq 0.4\%$) and/or are not short-lived episodes (for instance, the overall negative
655 trend regrouping CMBa-c accounts for a total duration of 1 Ma, Table 4).

656 Barrera and Savin (1999) noted that the $\delta^{13}C$ negative excursion of the lower
657 Maastrichtian is seen most markedly at southern polar Sites 689, 690 and 750. These authors
658 proposed two distinct mechanisms to explain this excursion : (1) at the global scale, an
659 increased ratio of organic to inorganic carbon in the input to the oceans driven by increased
660 weathering of organic-rich sediments exposed on continental shelves during the sea-level
661 drop, (2) in the southern ocean, a deepening of the oxygen minimum zone would reflect
662 increased oxidation of organic matter and an associated production of ^{13}C -depleted
663 bicarbonate which would have resulted in more pronounced negative values as observed in
664 the benthic foraminiferal profiles. However, these authors noted that a second sea-level drop
665 recorded in C30n (Haq et al., 1987 and Kominz et al., 2008) did not affect this ratio as
666 inferred from their $\delta^{13}C$ values in that interval. In the Late Cretaceous (Cenomanian to
667 Campanian), Jarvis et al. (2002, 2006) noted that the carbon-isotope reference curve for the
668 English Chalk was remarkably similar in shape to supposedly eustatic sea-level curves. They

669 concluded that both long-term and short-term $\delta^{13}\text{C}$ changes were controlled by sea-level
670 throughout these stages with increasing $\delta^{13}\text{C}$ values accompanying sea-level rise and
671 transgression, and decreasing $\delta^{13}\text{C}$ values characterizing sea-level fall and regression. This
672 relationship is explained by variations in epicontinental sea area affecting organic-matter
673 burial fluxes.

674 When taking into account the large uncertainty of the age-scale of the sea-level curve
675 for the Late Cretaceous (+/- 1Ma, Kominz et al., 2008), it is not currently possible to confirm
676 or infirm Jarvis' hypothesis on the relationship between variations of the sea-level and
677 variations of $\delta^{13}\text{C}$ in the Late Cretaceous (Fig. 10). More work is needed to reduce these
678 uncertainties and establish the evolution of regional sea-level changes.

679 Friedrich et al. (2009) interpreted the large carbon isotope perturbations of the CMB
680 and early Maastrichtian as a weakening of surface water stratification and increased
681 productivity in the southern high latitudes caused by ongoing cooling during the Late
682 Cretaceous. This would have led to the strengthening contribution of intermediate- to deep-
683 water production in the high southern latitudes.

684 Climate change might have also contributed to some of the observed $\delta^{13}\text{C}$ excursions.
685 In particular, in the late Maastrichtian, M4-(b) is coincident with the last occurrence of the
686 high-fertility species *Biscutum constans* (Fig. 9). This bio-event, which was also recorded in
687 the Tropical Atlantic and Pacific Oceans (Thibault and Gardin, 2010) could suggest a
688 decrease of surface-water fertility by the end of the Maastrichtian. In addition, M4-(b) occurs
689 during the acme of nannofossil warm-water species *Micula murus* which has been interpreted
690 as the expression of the end-Maastrichtian Deccan warming (Thibault and Gardin, 2006,
691 2007, 2010). This warming event has not been associated so far with any stratification of the
692 ocean and the pulse of volcanically derived CO_2 ($\delta^{13}\text{C} \approx -5\text{‰}$) associated with Deccan
693 volcanism would have contributed only to very small changes in the isotopic composition of

694 the oceans (Kump and Arthur, 1999). However, this global warming event might have
695 significantly reduced photosymbiotic activity (Abramovich and Keller, 2003) and caused an
696 ecological stress (Li and Keller, 1998a, 1998b; Abramovich and Keller, 2003), resulting in a
697 decrease of surface ocean productivity. Thus, the negative excursion M4-(b) may be the
698 expression of a global decrease in surface ocean productivity.

699

700 **6. Conclusions**

701

- 702 1) Combined calcareous plankton biostratigraphy, $\delta^{13}\text{C}$ stratigraphy, magneto- and
703 cyclostratigraphy of ODP Hole 762C has been established and shows that this site
704 had a nearly continuous sedimentation all along the upper Campanian–Maastrichtian
705 apart from a ~500 kyr gap identified in Chron C31n.
- 706 2) There is no disconformity in the lower Maastrichtian of the Exmouth Plateau contrary
707 to what stated in Howe et al. (2003). The observed higher-than-expected extinctions
708 of lower Maastrichtian nannofossil species, and the different stratigraphic orders of
709 nannofossil and foraminifera events as compared to “standard” Tethyan zonation,
710 are rather the result of diachronism and migration patterns between the Tethyan,
711 Transitional and Austral realms. These migration patterns could well be caused by
712 paleoceanographic reorganizations triggered by the prominent climatic changes of the
713 Campanian–Maastrichtian.
- 714 3) Results of the cyclostratigraphic approach tied to the astronomical calibration of the
715 Maastrichtian allowed a precise age-calibration of biostratigraphic events and of the
716 carbon-isotope profile.
- 717 4) Reduced sedimentation rates in the early Maastrichtian may be the response to either
718 reduced pelagic carbonate productivity, or either major global reorganizations of

- 719 bottom-currents leading to reduced sedimentation rates along the northwestern
720 margin of Australia.
- 721 5) Correlation of the calibrated $\delta^{13}\text{C}$ profile of Hole 762C to that of the Tercis section,
722 GSSP of the Campanian–Maastrichtian boundary, allows proposal of a precise age of
723 72.15 ± 0.05 Ma for this boundary considering an age of 66 Ma for the K-Pg boundary.
724 The total duration of the Maastrichtian stage is 6.15 ± 0.05 Ma.
- 725 6) The original CMB as defined by the base of the Boreal Belemnite zone *Belemnella*
726 *lanceolata* in northwest Germany is ~800 kyr older than the CMB as defined in the
727 GSSP of Tercis les Bains, which, in turn lies at the base of the *Belemnella obtusa*
728 zone.
- 729 7) The obtained chronostratigraphic framework of ODP Hole 762C is proposed as a
730 robust reference for the Indian Ocean and can serve as a basis for large-scale
731 correlation of $\delta^{13}\text{C}$ profiles and to test synchronism/diachronism of microfossil bio-
732 events throughout the Boreal, Tethyan, Transitional and Austral realms.

733

734 *Plate 1 and Plate 2 around here: format portrait full page*

735

736 Acknowledgements

737

738 We are grateful to Nathalie Labourdette, Damien Huygues and Vincent Gressier for technical
739 support and analytical help. Kipis to Julien Moreau. This research used samples provided by
740 the Ocean Drilling Program (ODP). ODP is sponsored by the US National Science
741 Foundation (NSF) and participating countries under the management of Joint Oceanographic
742 Institutions (JOI), Inc. Funding for this study was provided by Eclipse II Program, the Danish
743 National Foundation (FNU) and the Carlsberg Foundation. We warmly thank Silke Voigt and

744 Andy Gale for numerous fruitful discussions on Campanian–Maastrichtian stratigraphy as
745 well as Jim Ogg and an anonymous reviewer for their insightful and constructive reviews.

746

747 References

748

749 Abramovich, S., Keller, G., 2002. High stress late Maastrichtian paleoenvironment: inference
750 from planktonic foraminifera in Tunisia. *Palaeogeogr. Palaeoclimat. Palaeoecol.* 178,
751 145–164.

752 Abramovich, S., Keller, G., 2003. Planktonic foraminiferal response to the latest
753 Maastrichtian abrupt warm event: a case study from South Atlantic DSDP Site 525A.
754 *Mar. Micropaleontol.* 48, 225–249.

755 Apthorpe, M.C., 1979. Depositional history of the Upper Cretaceous of the Northwest shelf,
756 based upon Foraminifera. *The APPEA Journal* 19, 74–89.

757 Arthur, M. A., Dean, W.E., Pratt, L.M. 1988. Geochemical and climatic effects of increased
758 marine organic carbon burial at the Cenomanian/Turonian boundary, *Nature* 35, 714– 717.

759 Barchi, P., Bonnemaïson, M., Galbrun, B., Renard, M., 1997. Tercis (Landes, Sud-Ouest
760 France) : point stratotypique de la limite Campanien-Maastrichtien. Résultats
761 magnétostratigraphiques et premières données sur la nannoflore calcaire. *Bull. Soc. Géol.*
762 *France* 168, 133–142.

763 Barrera, E., Savin, S.M., 1999. Evolution of Campanian–Maastrichtian marine climates and
764 oceans. In: Barrera, E., Johnson, C.C. (Eds.), *Evolution of the Cretaceous Ocean-Climate*
765 *System. Geol. Soc. Am. Spec. Paper*, vol. 332, pp. 245–282.

766 Barrera, E., Savin, S.M., Thomas, E., Jones, C.E., 1997. Evidence for thermohaline-
767 circulation reversals controlled by sea level change in the latest Cretaceous. *Geology* 25,
768 715–718.

769 Batenburg, S.J., Sprovieri, M., Gale, A.S., Hilgen, F.J., Hüsing, S., Laskar, J., Liebrand, D.,
770 Lirer, F., Orue-Etxebarria, X., Pelosi, N., Smit, J., 2012. Cyclostratigraphy and
771 astronomical tuning of the Maastrichtian at Zumaia (Basque country, Northern Spain).
772 *Earth Planet. Sci. Lett.*, in press.

773 Birkelund, T., Hancock, J.M., Hart, M.B., Rawson, P.F., Remane, J., Robaszynski, F.,
774 Schmid, F., and Surlyk, F. 1984. Cretaceous stage boundaries Proposals. *Bulletin of the*
775 *Geological Society of Denmark* 33, 3–20.

776 Bown, P.R., 1998. *Calcareous Nannofossil Biostratigraphy*. British Micropaleontology
777 Society Publication Series. Chapman & Hall/Kluwer Academic Publishers, London, 328
778 pp.

779 Bralower, T.J., Siesser, W., 1992. Cretaceous calcareous nannofossil biostratigraphy of Sites
780 761, 762 and 763, Exmouth and Wombat Plateaus, northwest Australia. *Proc. ODP Sci.*
781 *Results* 122, 529-556.

782 Bralower, T.J., Leckie, R.M., Sliter, W.V., Thierstein, H.R., 1995. An integrated Cretaceous
783 microfossil biostratigraphy. In: Berggren, W.A., Kent, D.V., Aubry, M.-P., Hardenbol, J.
784 (Eds.), *Geochronology, Timescales and Global Stratigraphic Correlations*. SEPM Special
785 Publication 54, Tulsa, pp. 65–79.

786 Burnett, J.A. with contributions from Gallagher, L.T. & Hampton, M.J. 1998. Upper
787 Cretaceous. In: P.R. Bown (Ed.). *Calcareous Nannofossil Biostratigraphy*. British
788 Micropalaeontological Society Series. Chapman & Hall/Kluwer Academic Publishers,
789 London: 132–199.

790 Campbell, R.J., Howe, R.W., Rexilius, J.P., 2004. Middle Campanian–lowermost
791 Maastrichtian nannofossil and foraminiferal biostratigraphy of the northwestern
792 Australian margin. *Cretaceous Res.* 25, 827–864.

793 Cande, S.C., Kent, D.V., 1995. Revised calibration of the geomagnetic polarity timescale for
794 the late Cretaceous and Cenozoic. *J. Geophys. Res.* 100, 6093–6095.

795 Cerlings, T. E., Y. Wang, Quade, J., 1993. Expansion of C4 ecosystems as an indicator of
796 global ecological change in the late Miocene. *Nature* 361, 344– 345.

797 Chave, A.D., 1984, Lower Paleocene-Upper Cretaceous magnetostratigraphy, Sites 525, 527,
798 528, and 529, Deep Sea Drilling Project Leg 74, Init. Rep. DSDP 74, 525–531.

799 Cramer, B.S., 2001. Latest Palaeocene-earliest Eocene cyclostratigraphy: using core
800 photographs for reconnaissance geophysical logging. *Earth Planet. Sci. Lett.* 186, 231–
801 244.

802 Debajyoti, P., Skrzypek, G., Forizs, I., 2007. Normalization of measured stable isotopic
803 compositions to isotope reference scales – a review. *Rapid Commun. Mass Spectrom.* 21,
804 3006–3014.

805 Dickens, G.R., O'Neil, J.R., Rea, D.K., Owen, R.M., 1995. Dissociation of oceanic methane
806 hydrate as a cause of the carbon isotope excursion at the end of the Paleocene.
807 *Paleoceanography* 10, 965–971.

808 Föllmi, K.B., Godet, A., Bodin, S., Linder, P., 2006. Interactions between environmental
809 change and shallow water carbonate buildup along the northern Tethyan margin and their
810 impact on the Early Cretaceous carbon isotope record. *Paleoceanography* 21, PA4211,
811 doi:10.1029/2006PA001313.

812 Frank, T.D., Arthur, M.A., 1999. Tectonic forcings of Maastrichtian ocean-climate evolution.
813 *Paleoceanography* 14, 103-117.

814 Friedrich, O., Herrle, J.O., Hemleben, C., 2005. Climatic changes in the Late Campanian–
815 Early Maastrichtian: Micropaleontological and stable isotopic evidence from an
816 epicontinental sea. *J. Foraminiferal Res.* 35, 228–247.

817 Friedrich, O., Herrle, J.O., Wilson, P.A., Cooper, M.J., Erbacher, J., Hemleben, C., 2009.
818 Early Maastrichtian carbon cycle perturbation and cooling event: Implications from the
819 South Atlantic Ocean. *Paleoceanography* 24, PA2211, doi:10.1029/2008PA001654.

820 Galbrun, B., 1992. Magnetostratigraphy of Upper Cretaceous and lower Tertiary sediments,
821 Sites 761 and 762, Exmouth Plateau, northwest Australia. *Proc. ODP Sci. Results* 122,
822 699–716.

823 Gale, A.S., Jenkyns, H.C., Kennedy, W.J., Corfield, R.M., 1993. Chemostratigraphy versus
824 biostratigraphy: data from around the Cenomanian–Turonian boundary. *J. Geol. Soc.*
825 London 150, 29–32.

826 Gardin, S., Monechi, S., 2001. Calcareous Nannofossil distribution in the Tercis geological
827 site (Landes, SW France) around the Campanian-Maastrichtian boundary, in: Odin G.S.
828 (Ed.), *The Campanian–Maastrichtian stage boundary. Characterization at Tercis les Bains*
829 (France) and correlation with Europe and other continents. *Developments in*
830 *Palaeontology and Stratigraphy* 19, pp. 272–284.

831 Gardin, S., Odin, G.S., Bonnemaïson, M., Melinte, M., Monechi, S., von Salis, K., 2001.
832 Results of the cooperative study on the calcareous nannofossils across the Campanian-
833 Maastrichtian boundary at Tercis les Bains (Landes, France), in: Odin G.S. (Ed.), *The*
834 *Campanian–Maastrichtian stage boundary. Characterization at Tercis les Bains (France)*
835 *and correlation with Europe and other continents. Developments in Palaeontology and*
836 *Stratigraphy* 19, pp. 293–309.

837 Gardin, S., Galbrun, B., Thibault, N., Coccioni, R., Premoli Silva, I., 2012. Bio-
838 magnetochronology for the upper Campanian - Maastrichtian from the Gubbio area, Italy:
839 new results from the Contessa Highway and Bottaccione sections. *Newsl. Stratigr.* 45, in
840 press.

841 Golovchenko, X., Borella, P.E., O'Connell, S., 1992. Sedimentary cycles on the Exmouth
842 Plateau. Proc. ODP Sci. Results 122, 279–294.

843 Gradstein, F.M., Ogg, J.G., Smith, A.G., 2004. A Geologic Time Scale 2004, Cambridge
844 University Press, Cambridge, U.K., 500 pp.

845 Hancock, J.M., 1991. Ammonite time scales for the Cretaceous. Cretaceous Res. 12, 259–
846 291.

847 Haq, B.U., Hardenbol, J., Vail, P.R., 1987. Chronology of fluctuating Sea levels Since the
848 Triassic. Science 235, 1156–1167.

849 Haq et al., 1992. Site 762, Shipboard Scientific Party. Proc. ODP Init. Rep. 122, 213–288.

850 Hay, W.H., DeConto, R.M., Wold, C.N., Wilson, K.N., Voigt, S., Schulz, M., Rossby Wold,
851 A., Dullo, W.-C., Ronov, A.B., Balukhovskiy, A.N., Söding, E., 1999. Alternative global
852 Cretaceous paleogeography. In: Barrera, E., Johnson, C. C. (Eds.), Evolution of the
853 Cretaceous Ocean-Climate System: Boulder, Colorado, Geol. Soc. Am. Spec. Paper 332,
854 1–47.

855 Henriksson, A.S., 1993. Biochronology of the terminal Cretaceous calcareous nannofossil
856 Zone of *Micula prinsii*. Cretaceous Res. 14, 59–68.

857 Hesselbo, S. P., Gröcke, D.R., Jenkyns, H.C., Bjerrum, C.J., Farrimond, P., Bell, H.S.M.,
858 Green, O.R., 2000. Massive dissociation of gas hydrate during a Jurassic oceanic anoxic
859 event. Nature 406, 392–395.

860 Hilgen, F. J., Kuiper, K. F., and Lourens, L. J. (2010). Evaluation of the astronomical time
861 scale for the Paleocene and earliest Eocene. Earth Planet. Sci. Lett. 300, 139–151.

862 Howe, R.W., Campbell, R.J., Rexilius, J.P., 2003. Integrated uppermost Campanian–
863 Maastrichtian calcareous nannofossil and foraminiferal biostratigraphic zonation of the
864 northwestern margin of Australia. Journal of Micropalaeontology 22, 29–62.

865 Huang, Z., Boyd, R., O'Connell, S., 1992. Upper Cretaceous cyclic sediments from Hole
866 762C, Exmouth Plateau, northwest Australia. *Proc. ODP Sci. Results* 122, 259–278.

867 Huber, B.T., 1992a. Paleobiogeography of Campanian–Maastrichtian foraminifera in the
868 southern high latitudes. *Palaeogeogr. Palaeoclimatol. Palaeoecol.* 92, 325–360.

869 Huber, B.T., 1992b. Upper Cretaceous planktic foraminiferal zonation for the Austral Realm.
870 *Mar. Micropaleontol.* 20, 107–128

871 Huber, B.T., Watkins, D.K., 1992. Biogeography of Campanian–Maastrichtian calcareous
872 plankton in the region of the Southern Ocean: Paleogeographic and Paleoclimatic
873 implications. In: Kennett, J.P., Warnke, D.A. (Eds.), *The Antarctic Paleoenvironment: A
874 Perspective on Global Change*. American Geophysical Union, Antarctic Research Series
875 56, Washington, pp. 31–60.

876 Husson, D., Galbrun, B., Laskar, J., Hinnov, L., Thibault, N., Gardin, S., Locklair, R.E., 2011.
877 Astronomical calibration of the Maastrichtian (late Cretaceous). *Earth Planet. Sci. Lett.*
878 305, 328–340.

879 Husson, D., Galbrun, B., Thibault, N., Gardin, S., Huret, E., Coccioni, R., 2012. Astronomical
880 duration of polarity Chron C31r (Lower Maastrichtian): cyclostratigraphy of ODP Site
881 762 (Indian Ocean) and the Contessa Highway section (Gubbio, Italy). *Geol. Mag.* 149,
882 345–351.

883 Immenhauser, A., Della Porta, G. Kenter, J. A. M., Bahamonde, J.R., 2003. An alternative
884 model for positive shifts in shallow-marine carbonate $\delta^{13}\text{C}$ and $\delta^{18}\text{O}$. *Sedimentology* 50,
885 953–959.

886 Ion, J., Odin, G.S., 2001. Planktonic foraminifera from the Campanian-Maastrichtian at
887 Tercis les Bains (Landes, France). In: Odin, G.S. (Ed.), *The Campanian-Maastrichtian
888 stage boundary: characterisation at Tercis les Bains (France): correlation with Europe and*

889 other continents. *Developments in Palaeontology and Stratigraphy Series 19*, Elsevier
890 Sciences Publ. Amsterdam, 349-378.

891 Jarvis, I., Mabrouk, A., Moody, R.T.J., de Cabrera, S., 2002. Late Cretaceous (Campanian)
892 carbon isotope events, sea-level change and correlation of the Tethyan and Boreal realms.
893 *Palaeogeogr. Palaeoclimatol. Palaeoecol.* 188, 215–248.

894 Jarvis, I., Gale, A.S., Jenkyns, H.C., Pearce, M.A., 2006. Secular variation in Late Cretaceous
895 carbon isotopes: a new $\delta^{13}\text{C}$ carbonate reference curve for the Cenomanian–Campanian
896 (99.6–70.6 Ma). *Geol. Mag.* 143, 561–608.

897 Jenkyns, H.C., Gale, A.S., Corfield, R.M., 1994. Carbon- and oxygen-isotope stratigraphy of
898 the English Chalk and Italian Scaglia and its palaeoclimatic significance. *Geol. Mag.* 131,
899 1–34.

900 Jenkyns, H.C., Mutterlose, J., Sliter, W.V., 1995. Upper Cretaceous carbon- and oxygen-
901 isotope stratigraphy of deep-water sediments from the North-Central Pacific (Site 869,
902 Flank of Pikini-Wodejebato, Marshall Islands). *Proc. ODP Sci. Results* 143, 105-108.

903 Johnson, C.C., Barron, E.J., Kauffman, E.G., Arthur, M.A., Fawcett, P.J., Yasuda, M.K.,
904 1996. Middle Cretaceous reef collapse linked to ocean heat transport. *Geology* 24, 376–
905 380.

906 Kominz, M.A., Browning, J.V., Miller, K.G., Sugarman, P.J., Mizintsevaw, S., Scotese, C.R.,
907 2008. Late Cretaceous to Miocene sea-level estimates from the New Jersey and Delaware
908 coastal plain coreholes: an error analysis. *Basin Res.* 20, 211–226.

909 Kuiper, K.F., Deino, A., Hilgen, F.J., Krijgsman, W., Renne, P.R., and Wijbrans, J.R., 2008.
910 Synchronizing rock clocks of earth history. *Science* 320, 500-504.

911 Kump, L. R., Arthur, M.A., 1999. Interpreting carbon-isotope excursions: Carbonates and
912 organic matter. *Chem. Geol.* 161, 181– 198.

913 Laskar, J., Fienga, A., Gastineau, M., Manche, H., 2011. La2010: a new orbital solution for
914 the long-term motion of the Earth. *Astronomy and Astrophysics* 532, A89, 1–15, DOI:
915 <http://dx.doi.org/10.1051/0004-6361/201116836>.

916 Landman, N.H., Waage, K.M., 1993. Scaphitid ammonites of the Upper Cretaceous
917 (Maastrichtian) Fox Hills formation in South Dakota and Wyoming, *Bulletin of the*
918 *American Museum of Natural History* 215, 1–257.

919 Lees, J.A., 2002. Calcareous nannofossils biogeography illustrates palaeoclimate change in
920 the Late Cretaceous Indian Ocean. *Cretaceous Res.* 23, 537–634.

921 Lees, J.A., Bown, P.R., 2005. Upper Cretaceous calcareous nannofossil biostratigraphy, ODP
922 Leg 198 (Shatsky Rise, northwest Pacific Ocean). *Proc. Ocean Drill. Program Sci. Results*
923 198, 1–60. doi:10.2973/odp.proc.sr.198.114.2005.

924 Lewy, Z., Odin, G.S., 2001. Magnetostratigraphy across the Campanian-Maastrichtian
925 boundary at Tercis les Bains in comparison with northern Germany, the Apennines
926 (Central Italy) and North America; biostratigraphical and Central Italy) and North
927 America; biostratigraphical and geochronological constraints. In: Odin, G.S. (Ed.), *The*
928 *Campanian-Maastrichtian stage boundary: characterisation at Tercis les Bains (France):*
929 *correlation with Europe and other continents. Developments in Palaeontology and*
930 *Stratigraphy Series 19, Elsevier Sciences Publ. Amsterdam, 175-183.*

931 Li, L., Keller, G., 1998a. Maastrichtian climate, productivity and faunal turnovers in planktic
932 foraminifera in South Atlantic DSDP sites 525A and 21. *Mar. Micropaleontol.* 33, 55–86.

933 Li, L., Keller, G., 1998b. Abrupt deep-sea warming at the end of the Cretaceous. *Geology* 26,
934 995–998.

935 Li, L., Keller, G., 1999. Variability in Late Cretaceous and deep waters: evidence from stable
936 isotopes. *Mar. geol.* 161, 171–190.

937 MacLeod, K.G., Huber, B.T., Ward, P.D., 1996. The biostratigraphy and paleobiogeography
938 of Maastrichtian inoceramids. In: Ryder, G., Fastovsky, D., Gartner, S. (Eds.), *The*
939 *Cretaceous–Tertiary Event and Other Catastrophes in Earth History*. Geol. Soc. Am. Spec.
940 Paper 307, Boulder, pp. 361–373.

941 Manivit, H., 1984. Paleogene and Upper Cretaceous calcareous nannofossils from Deep Sea
942 Drilling Project Leg 74. *Init. Rep. Deep Sea Drill. Proj. 74*, 475–499.

943 McArthur, J.M., Kennedy, W.J., Gale, A.S., Thirlwall, M.F., Chen, M., Burnett, J., Hancock,
944 J.M., 1992. Strontium isotope stratigraphy in the Late Cretaceous: intercontinental
945 correlation of the Campanian/Maastrichtian boundary. *Terra Nova* 4, 385–393.

946 McArthur, J.M., Kennedy, W.J., Chen, M., Thirlwall and M.F. Gale, A.S., 1994. Strontium
947 isotope stratigraphy for Late Cretaceous time: Direct numerical calibration of the Sr
948 isotope curve based on the US Western Interior. *Palaeogeogr. Palaeoclimatol. Palaeoecol.*
949 108, 95–119.

950 Miller, K.G., Barrera, E., Olsson, R.K., Sugarman, P.J. and Savin, S.M., 1999. Does ice drive
951 early Maastrichtian eustasy? *Geology* 27, 783–786.

952 Mitchell, S.F., Ball, J.D., Crowley, S.F., Marshall, J.D., Paul, C.R.C., Veltkamp, C.J., Samir,
953 A., 1997. Isotope data from cretaceous chalks and foraminifera: Environmental or
954 diagenetic signals? *Geology* 25, 691–694.

955 Niebuhr, B., Esser, K., 2003. Late Campanian and Early Maastrichtian ammonites from the
956 white chalk of Krons Moor (northern Germany) – taxonomy and stratigraphy. *Acta Geol.*
957 *Pol.* 53, 257–281.

958 Odin, G.S., 1996, Observations stratigraphiques sur le Maastrichtien. Arguments pour la
959 localisation et la corrélation du Point Stratotype Global de la limite Campanien-
960 Maastrichtien, *Bull. Soc. Géol. France* 167, 637–643.

961 Odin, G.S., 2001. The Campanian-Maastrichtian stage boundary: characterisation at Tercis les
962 Bains (France): correlation with Europe and other continents. *Developments in*
963 *Palaeontology and Stratigraphy Series 19*, Elsevier Sciences Publ. Amsterdam, 910 p.

964 Odin, G.S., and Amorosi, A., 2001. Interpretative reading of the Campanian-Maastrichtian
965 deposits at Tercis les Bains: sedimentary breaks, rhythms, accumulation rate, sequences.
966 In: Odin, G.S. (Ed.), *The Campanian-Maastrichtian stage boundary: characterisation at*
967 *Tercis les Bains (France): correlation with Europe and other continents. Developments in*
968 *Palaeontology and Stratigraphy Series 19*, Elsevier Sciences Publ. Amsterdam, 125-135.

969 Odin, G.S. and Lamaurelle, M.A., 2001. The global Campanian-Maastrichtian stage
970 boundary. *Episodes* 24, 229–237.

971 Olsson, R.K., Wright, J.D., Miller, K.G., 2001. Paleobiogeography of *Pseudotextularia*
972 *elegans* during the latest Maastrichtian global warming event. *J. Foraminiferal Res.* 31,
973 275–282.

974 Pälke, H., Norris, R.D., Herrle, J.O., Wilson, P.A., Coxall, H.K., Lear, C.H., Shackleton,
975 N.J., Tripathi, A.K., Wade, B.S., 2006. The heartbeat of the Oligocene climate system.
976 *Science* 314, 1894–1898.

977 Panchuk, K. M., Holmden, C., Kump, L.R., 2005. Sensitivity of the epeiric sea carbon
978 isotope record to local-scale carbon cycle processes: Tales from the Mohawkian Sea,
979 *Palaeogeogr. Palaeoclimat. Palaeoecol.* 228, 320–337.

980 Panchuk, K. M., C. E. Holmden, Leslie, S.A., 2006. Local controls on carbon cycling in the
981 Ordovician midcontinent region of North America, with implications for carbon isotope
982 secular curves. *J. Sediment. Res.* 76, 200– 211.

983 Perch-Nielsen, K., 1985. Mesozoic calcareous nannofossils. In: Bolli, H., S et al. (Editors),
984 *Plankton Stratigraphy*. Cambridge University Press, pp. 329–426.

- 985 Petrizzo, M.R., 2000. Upper Turonian–lower Campanian planktonic foraminifera from
986 southern mid-high latitudes (Exmouth Plateau, NW Australia): biostratigraphy and
987 taxonomic notes. *Cretaceous Res.* 21, 479–505.
- 988 Petrizzo, M.R., 2003. Late Cretaceous planktonic foraminiferal bioevents in the Tethys and in
989 the Southern Ocean: an overview. *J. Foraminiferal Res.* 33, 330–337.
- 990 Premoli Silva, I., Sliter, W.V., 1994. Cretaceous planktonic foraminiferal biostratigraphy and
991 evolutionary trends from the Bottaccione section, Gubbio, Italy. *Palaeontogr. Ital.* 82, 1–
992 89.
- 993 Renne, P.R., Mundil, R., Balco, G., Min, K., Kudwig, K.R., 2010. Joint determination of ^{40}K
994 decay constants and $^{40}\text{Ar}^*/^{40}\text{Ar}$ for the Fish Canyon sanidine standard, and improved
995 accuracy for $^{40}\text{Ar}/^{39}\text{Ar}$ geochronology. *Geochim. Cosmochim. Acta.*, doi:
996 10.1016/j.gca.2010.06.017.
- 997 Rexilius, J.P., 1984. Late Cretaceous foraminiferal and calcareous nannoplankton
998 biostratigraphy, Southwestern Australian Margin. PhD Thesis. Department of Geology
999 and Geophysics, The University of Western Australia, 291p.
- 1000 Scholle, P. A., Arthur, M.A., 1980. Carbon isotope fluctuations in Cretaceous pelagic
1001 limestones: Potential stratigraphic and petroleum exploration tool. *Am. Assoc. Petrol.*
1002 *Geol. Bull.* 64, 67–87.
- 1003 Schönfeld, J., Schulz, M.-G., Arthur, M.A., Burnett, J., Gale, A.S., Hambach, U., Hansen,
1004 H.J., Kennedy, W.J., Rasmussen, K.L., Thirlwall, M.F., Wray, D.S., 1996. New results on
1005 biostratigraphy, paleomagnetism, geochemistry and correlation from the standard section
1006 for the Upper Cretaceous white chalk of northern Germany (Lägerdorf-Kronsmoor-
1007 Hemmoor). *Mitteilungen des Geologisch-Paläontologischen Institutes der Universität*
1008 *Hamburg* 77, 545–575.

1009 Schrag, D.P., DePaolo, D.J., Richter, F.M, 1995. Reconstructing past sea surface
1010 temperatures: correcting for diagenesis of bulk marine carbon. *Geochim. Cosmochim. Ac.*
1011 59, 2265–2278.

1012 Shafik, S., 1990. Late Cretaceous nannofossil biostratigraphy and biogeography of the
1013 Australian western margin. Bureau of Mineral Resources, Geology and Geophysics,
1014 Report 295, 1–164.

1015 Shafik, S., 1998. Problems with the Cretaceous biostratigraphic system of Australia: time for
1016 a review. *Australian Geological Survey Organisation Research Newsletter* 28, 12–14.

1017 Swart, P. K., Eberli, G., 2005. The nature of the $\delta^{13}\text{C}$ of periplatform sediments: Implications
1018 for stratigraphy and the global carbon cycle, *Sedim. Geol.* 175, 115– 129.

1019 Thibault, N., Gardin, S., 2006. Maastrichtian calcareous nannofossil biostratigraphy and
1020 paleoecology in the Equatorial Atlantic (Demerara Rise, ODP Leg 207 Hole 1258A). *Rev.*
1021 *Micropaleontol.* 49, 199–214.

1022 Thibault, N., Gardin, S., 2007. The late Maastrichtian nannofossil record of climate change in
1023 the South Atlantic DSDP Hole 525A. *Mar. Micropaleontol.* 65, 163–184.

1024 Thibault, N., Gardin, S., Galbrun, B., 2010. Latitudinal migration of calcareous nannofossil
1025 *Micula murus* in the Maastrichtian: Implications for global climate change. *Geology* 38,
1026 203–206.

1027 Thibault, N., Schovsbo, N., Harlou, R., Stemmerik, L., Surlyk, F., 2011. An age-calibrated
1028 record of upper Campanian – Maastrichtian climate change in the Boreal Realm. Abstract,
1029 2011 Fall Meeting, AGU, San Francisco, Calif., 5-9 Dec.

1030 Thibault, N., Harlou, R., Schovsbo, N., Schiøler, P., Minoletti, F., Galbrun, B., Lauridsen,
1031 B.W., Sheldon, E., Stemmerik, L., Surlyk, F., 2012. Upper Campanian–Maastrichtian
1032 nannofossil biostratigraphy and high-resolution carbon-isotope stratigraphy of the Danish
1033 Basin: towards a standard $\delta^{13}\text{C}$ curve for the Boreal Realm. *Cretaceous Res.* 33, 72–90.

- 1034 Thomson, D.J., 1982. Spectrum estimation and harmonic analysis. *Inst. Electr. And Electron.*
1035 *Eng. Proc.* 70, 1055–1096.
- 1036 Voigt, S., 2000. Cenomanian–Turonian composite $\delta^{13}\text{C}$ curve for Western and Central
1037 Europe: the role of organic and inorganic carbon fluxes. *Palaeogeogr. Palaeoclimatol.*
1038 *Palaeoecol.* 160, 91–104.
- 1039 Voigt, S., Schönfeld, J., 2010. Cyclostratigraphy of the standard section for the Cretaceous
1040 white chalk of northern Germany, Lägerdorf-Kronsmoor: a late Campanian – early
1041 Maastrichtian orbital time scale. *Palaeogeogr. Palaeoclimatol. Palaeoecol.* 287, 67–80.
- 1042 Voigt, S., Friedrich, O., Norris, R.D., Schönfeld, J., 2010. Campanian – Maastrichtian carbon
1043 isotope stratigraphy: shelf–ocean correlation between the European shelf sea and the
1044 tropical Pacific Ocean. *Newsl. Stratigr.* 44, 57–72.
- 1045 Voigt, S., Gale, A.S., Jung., C., Jenkyns, H.C., 2012. Global correlation of Upper
1046 Campanian–Maastrichtian successions using carbon-isotope stratigraphy: development of
1047 a new Maastrichtian timescale. *Newsl. Stratigr.* 45, in press.
- 1048 Weedon, G.P., 2003. Time series analysis and cyclostratigraphy: Examining stratigraphic
1049 records of environmental cycles: Cambridge, UK Cambridge University Press, 259 p.
- 1050 Weissert, H., 1989. C-isotope stratigraphy, a monitor of paleoenvironmental change: a case
1051 study from the Early Cretaceous. *Surv. Geophys.* 10, 1-61.
- 1052 Weissert, H., Erba, E., 2004. Volcanism, CO₂ and palaeoclimate: A late Jurassic-early
1053 Cretaceous carbon and oxygen isotope record. *Journ. Geol. Soc. London* 161, 695– 702.
- 1054 Weissert, H., Lini, A., Föllmi, K.B., Kuhn, O., 1998. Correlation of Early Cretaceous carbon
1055 isotope stratigraphy and platform drowning events: A possible link? *Palaeogeogr.,*
1056 *Palaeoclimat., Palaeoecol.* 137, 189–203.

1057 Westerhold, T., Röhl, U., Raffi, I., Fornaciari, E., Monechi, S., Reale, V., Bowles, J., Evans,
1058 H.F., 2008. Astronomical calibration of the Paleocene time. *Palaeogeogr. Palaeoclimatol.,*
1059 *Palaeoecol.* 257, 377–403.

1060 Wonders, A.A.H., 1992. Cretaceous planktonic foraminiferal biostratigraphy, Leg 122,
1061 Exmouth Plateau, Australia. *Proc. ODP, Sci. Results* 122, 587-600.

1062 Young, J.R., Bown, P.R., 1997. Higher classification of calcareous nannoplankton. *J.*
1063 *Nannoplankton Res.* 19, 15-20.

1064 Zepeda, M.A., 1998. Planktonic foraminiferal diversity, equitability and biostratigraphy of the
1065 uppermost Campanian-Maastrichtian, ODP Leg 122, Hole 762C, Exmouth Plateau, NW
1066 Australia, eastern Indian Ocean. *Cretaceous Res.* 19, 117–152.

1067

1068 Captions to figures

1069

1070 Figure 1 : A. Palaeogeographic reconstruction of the Southern Hemisphere for the upper
1071 Campanian-lower Maastrichtian showing the location of ODP Hole 762C, DSDP Hole 525A,
1072 and the inferred palaeobiogeographical boundaries between the Austral, Transitional and
1073 Tethyan provinces (from Huber, 1992a). B. Map of Europe showing other important locations
1074 of Campanian-Maastrichtian sections. G: Gubbio, LKH: Lägerdorf – Kronsmoor – Hemmoor,
1075 M: Maastricht, N: Norfolk, R: Rørdal, S: Stevns-1, T: Tercis les Bains.

1076

1077 Figure 2 : Magnetostratigraphy, bulk-carbonate $\delta^{13}\text{C}$ profile, planktic foraminifer and
1078 nannofossil bio-events in ODP Hole 762C, with inferred biozonations of Howe et al. (2003)
1079 and Campbell et al. (2004) for planktic foraminifera and Burnett (1998) for calcareous
1080 nannofossils. (a) Revised in this study from data published by Galbrun (1992). (b) Planktic
1081 foraminifer transitional biozonation from Zepeda (1998). (c) Data from Howe et al. (2003).

1082 (d) This study. (e) Data from Campbell et al. (2004). C/F: sudden change of abundance from
1083 common to frequent only.

1084

1085 Figure 3 : Illustration of an ODP core photograph (core 48X) from the early Maastrichtian of
1086 Hole 762C. One hundred kyr eccentricity cycles e_{10039} to e_{10055} are identified on the core and
1087 bracketed between the “X”. A few obvious precession cycles are shown (P). These precession
1088 cycles are also expressed on the amplitude spectrograms of Figure 4 in the interval between
1089 604 and 610 ambsf.

1090

1091 Figure 4 : (a) Gray scale log reflectance. The presented signal has been filtered for cracks and
1092 lighting effects. (b) MTM power spectra of the gray scale log for the stratigraphical intervals
1093 550-593 ambsf and 593-638 ambsf. (c) Amplitude spectrograms for the studied interval. The
1094 shaded area corresponds to a “strange” interval with disturbance (D.) caused by numerous
1095 cracks in the cores which hinder the identification of clear 405 kyr eccentricity cycles.

1096

1097 Figure 5 : Cyclostratigraphic age-model for the upper Campanian-Maastrichtian of ODP Hole
1098 762C. The counting of 100 and 405 kyr eccentricity cycles is here based on the 100 kyr filter
1099 output extracted from the original gray-scale log reflectance. 405 kyr cycles are thus hand-
1100 counted by regroupment of 100 kyr cycles. From the base of C31n to the top of C33n, this
1101 counting corresponds fairly well to the extracted 405 kyr filter output (Figs. 7–10). The
1102 identified Campanian–Maastrichtian boundary level lies within 100 kyr eccentricity cycle
1103 e_{10062} which provides an age of 72.15 ± 0.05 Ma for the CMB (with a K-Pg boundary at 66
1104 Ma) and a total duration of 6.15 ± 0.05 Ma for the Maastrichtian stage.

1105

1106 Figure 6 : Cross-plot of carbon- and oxygen-isotope ratios for bulk samples analyzed from the
1107 Maastrichtian section of ODP Hole 762C. There is no significant correlation between the two
1108 sets of values.

1109

1110 Figure 7: Correlation of the age-calibrated $\delta^{13}\text{C}$ profile of ODP Hole 762C with the $\delta^{13}\text{C}$
1111 profile of Tercis les Bains, GSSP of the Campanian–Maastrichtian boundary, and the Gubbio
1112 composite section. (a) This study. PF datums are in bold and PF zones correspond to the
1113 transitional biozonation of Zepeda (1998). (b) All references on planktic foraminiferal (PF)
1114 and nannofossil biostratigraphic datums of Tercis les Bains can be found in Voigt et al.
1115 (2012). The first occurrences of planktic foraminifers *C. contusa* and *T. scotti* reported for the
1116 Tercis les Bains section are not reliable and thus not presented here (I. Premoli Silva in
1117 Gardin et al., 2012). (c) The Gubbio composite presented here was built using the $\delta^{13}\text{C}$
1118 records of the Bottaccione and Contessa sections presented in Voigt et al. (2012) and
1119 corresponding biostratigraphic datums of Gardin et al. (2012). (d) 405 kyr filter after Husson
1120 et al. (2011). Only the 100 kyr filtering could be used for magnetochrons C29r to C30r in
1121 Hole 762C, 405 kyr eccentricity cycles of this interval (in grey) are thus hand counted by
1122 regroupment of four 100 kyr cycles.

1123

1124 Figure 8: Correlation of $\delta^{13}\text{C}$ profiles between ODP Hole 762C (Indian Ocean), Stevns-1
1125 (Danish Basin), and Lägerdorf – Kronsmoor – Hemmoor composite section (LKH, Northwest
1126 Germany). (a) This study. (b) After Husson et al. (2011). Only the 100 kyr filtering could be
1127 used for magnetochrons C29r to C30r in Hole 762C, 405 kyr eccentricity cycles of this
1128 interval (in grey) are thus hand counted by regroupment of four 100 kyr cycles. (c) Thibault et
1129 al. (2012). (d) Voigt et al. (2010). (e) 405 kyr filter of CaCO_3 data and corresponding
1130 numbering of cycles for Boreal Campanian and Maastrichtian stages after Voigt and

1131 Schönfeld (2010). (f) Nannofossil datums by Burnett in Schönfeld et al. (1996). Belemnite
1132 zones are: polypl = *polyplucum*, gri/gra = *grimmensis/granulosis*, lan = *lanceolata*, p =
1133 *pseudoobtusata*, obt = *obtusata*, cimb = *cimbrica*, fas = *fastigata*, teg/jun = *tegulatus/junior*,
1134 arg/jun = *argentea/junior*, da = *danica*, ba/da = *baltica/danica*. The Boreal CMB as defined
1135 by belemnite zones in LKH section corresponds to the base of $\delta^{13}\text{C}$ event CMBa and thus
1136 shows a discrepancy of ca. two 405 kyr cycles with the CMB as defined in ODP Hole 762C
1137 within $\delta^{13}\text{C}$ event CMBc by comparison with the GSSP of Tercis les Bains.

1138

1139 Figure 9: Correlation of $\delta^{13}\text{C}$ profiles between ODP Hole 762C (Indian Ocean) and DSDP
1140 Hole 525A (South Atlantic). (a) Husson et al. (2011), (b) Thibault and Gardin (2007), (c)
1141 Manivit (1984), (d) Li and Keller (1998a).

1142

1143 Figure 10: Age-calibrated bulk-carbonate $\delta^{13}\text{C}$ profile and variations of the sedimentation rate
1144 in ODP Hole 762C vs variations of the sea-level as estimated in Miller et al. (2005), Kominz
1145 et al. (2008) and Haq et al. (1987).

1146

1147 Table 1: Top depths, sub-bottom depths, estimated absolute ages and error margins of
1148 calcareous nannofossil, planktic and benthic foraminifera bio-events in ODP Hole 762C. (a)
1149 calcareous nannofossil bio-events, this study. (b) planktic foraminiferal bio-events, Howe et
1150 al. (2003). (c) benthic foraminiferal bio-events, Howe et al. (2003). (d) planktic foraminiferal
1151 bio-events, Campbell et al. (2004). (e) calcareous nannofossil bio-events, Campbell et al.
1152 (2004).

1153

1154 Table 2: Depth and estimated ages (2a), and mean durations (2b) of uppermost Cretaceous
1155 magnetochrons in ODP Hole 762C and comparison with the standard Geological Time Scale

1156 (Gradstein et al., 2004). Table 2a modified after Husson et al. (2011). Note that the durations
1157 of C29r to C30n at ODP Hole 762C (2b) are consistent with the astronomical calibration of
1158 Husson et al. (2011). (*) The duration of chron C30r is doubtful because the base of this
1159 chron falls very near the identified 500 kyr gap and the cyclostratigraphic signal is distorted
1160 here (Fig. 5). Magnetostratigraphic durations and ages of upper Maastrichtian chron boundaries
1161 provided in Husson et al. (2011) are more precise with lower uncertainties and are rather
1162 adopted here for the chronostratigraphic framework of Figures 7-10. Magnetostratigraphic durations
1163 and ages of upper Campanian–lower Maastrichtian chron boundaries are based on Hole 762C
1164 in Husson et al. (2011). Comparison of these durations with the standard marine magnetic
1165 model is discussed in Husson et al. (2011).

1166

1167 Table 3: Description, top and bottom depths of $\delta^{13}\text{C}$ events in ODP Hole 762C. CMB:
1168 Campanian–Maastrichtian boundary.

1169

1170 Table 4: Top depths, sub-bottom depths, estimated absolute ages and durations of $\delta^{13}\text{C}$ events
1171 in ODP Hole 762C.

1172

1173 Plate 1: Calcareous nannofossils from the upper Campanian–Maastrichtian of ODP Hole
1174 762C. 1, *Ahmuellerella octoradiata*, 53X-7, 1–2 cm. 2, *Amphizygus brooksii*, 49X-1, 61–62
1175 cm. 3, *Biscutum coronum*, 44X-7, 14–15 cm. 4, *Biscutum constans*, 44X-4, 110–111 cm. 5,
1176 *Biscutum magnum*, 49X-1, 61–62 cm. 6, *Broinsonia parca constricta*, 49X-5, 124–125 cm. 7,
1177 *Broinsonia parca parca*, 55X-1, 66–67 cm. 8, *Calculites obscurus*, 51X-4, 11–12 cm. 9,
1178 *Ceratolithoides aculeus*, 50X-4, 101–102 cm. 10, *Ceratolithoides indiensis*, 43X-1, 33–34
1179 cm. 11, *Ceratolithoides kamptneri*, 44X-3, 108–109 cm. 12 *Cribracorona gallica*, 43X-1, 33–
1180 34 cm. 13, *Cribrosphaerella daniae*, 43X-1, 33–34 cm. 14, *Discorhabdus ignotus*, 49X-5, 35–

1181 36 cm. 15, *Eiffellithus angustus*, 52X-3, 77–78 cm. 16, *Eiffellithus eximius*, 54X-7, 20–21 cm.
 1182 17, *Lithraphidites praequadratus*, 43X-1, 33–34 cm. 18, *Lithraphidites quadratus*, 44X-4,
 1183 110–111 cm. 19, *Micula murus*, 43X-2, 33–34 cm. 20, *Micula praemurus*, 43X-2, 83–84 cm.
 1184 21, *Micula prinsii*, 43X-2, 33–34 cm. 22, *Micula prinsii*, 43X-1, 33–34 cm. 23,
 1185 *Monomarginatus quaternarius*, 49X-2, 82–83 cm. 24, *Nephrolithus frequens*, 43X-1, 33–34
 1186 cm. 25, *Petrarhabdus copulatus*, 49X-1, 9–10 cm. 26 and 27, *Petrarhabdus copulatus* (same
 1187 specimen), 49X-5, 35–36 cm. 28, *Petrarhabdus vietus* 48X-4, 54–55 cm. 29, *Prediscosphaera*
 1188 *mgayae*, 49X-1, 9–10 cm. 30, *Pseudomicula quadrata*, 43X-3, 66–67 cm. 31, *Quadrum*
 1189 *gartneri*, 50X-2, 11–12 cm. 32, *Quadrum svabenicka*, 51X-4, 11–12 cm. 33, *Reinhardtites*
 1190 *anthophorus*, 54X-6, 60–62 cm. 34, *Reinhardtites elegans*, 51X-6, 35–36 cm.

1191

1192 Plate 2: Calcareous nannofossils from the upper Campanian–Maastrichtian of ODP Hole
 1193 762C. 1, *Reinhardtites levis*, 51X-4, 11–12 cm. 2, *Rotelapillus laffittei*, 49X-1, 61–62 cm. 3,
 1194 *Stoverius* cf. *S. achylosus*, 48X-6, 104–105 cm. 4, *Stoverius coangustatus*, 49X-2, 82–83 cm.
 1195 5, *Stoverius coangustatus*, 50X-4, 101–102 cm. 6, *Tortolithus hallii*, 53X-3, 101–102 cm. 7,
 1196 *Tortolithus hallii*, 54X-7, 20–21 cm. 8, *Tranolithus orionatus*, 49X-4, 105–106 cm. 9,
 1197 *Tranolithus orionatus*, 55X-1, 66–67 cm. 10, *Tranolithus stemmerikii*, 50X-5, 100–101 cm.
 1198 11, *Tranolithus stemmerikii*, 55X-1, 66–67 cm. 12, *Uniplanarius gothicus*, 49X-5, 35–36 cm.
 1199 13, *Uniplanarius gothicus*, 49X-3, 104–105 cm. 14, *Uniplanarius sissinghii* (very rare), 50X-
 1200 3, 10–11 cm. 15, *Uniplanarius sissinghii*, 52X-3, 77–78 cm. 16, *Uniplanarius trifidus* short-
 1201 rayed, 51X-3, 10–11 cm. 17, *Uniplanarius trifidus* medium-rayed, 49X-3, 89–90 cm. 18,
 1202 *Uniplanarius trifidus* long-rayed (very rare), 52X-3, 77–78 cm. 19, *Watznaueria manivittiae*
 1203 sensu stricto, 55X-1, 66–67 cm. 20, *Watznaueria manivittiae* sensu lato, 49X-4, 105–106 cm.
 1204 21, *Zeugrhabdotus bicrescenticus* (big form), 52X-6, 83–85 cm. 22, *Zeugrhabdotus*
 1205 *bicrescenticus* (small form), 54X-1, 138–139 cm. 23, *Zeugrhabdotus diplogrammus*, 50X-1,

1206 10–11 cm. 24, *Zeugrhabdotus diplogrammus*, 49X-3, 104–105 cm. 25, *Zeugrhabdotus*
1207 *erectus*, 49X-3, 38–39 cm. 26, curved spine, 53X-1, 12–13 cm. 27, curved spine, 52X-2, 112–
1208 113 cm.

1209

1210 Appendix 1: Values of inclination, paleomagnetic interpretation and additional remarks for
1211 the upper Campanian–Maastrichtian of ODP Hole 762C.

1212

1213 Appendix 2: Stratigraphic distribution of key and potential stratigraphic calcareous
1214 nannofossil markers in the upper Campanian-Maastrichtian of ODP Hole 762C. M: moderate
1215 preservation, P: poor preservation.

1216

1217 Appendix 3: Alphabetical list of calcareous nannofossil species considered in this study.

1218

1219 Appendix 4: Grey level values obtained for core photographs used for cyclostratigraphy.

1220 These data correspond to a resampling at a step of 1 cm. Adjusted depths (ambsf) and
1221 equivalent original depths (mbsf) are given along with cores, sections and identified 100 kyr
1222 and 405 kyr eccentricity cycles.

1223

1224 Appendix 5: Measured and standardized bulk carbonate $\delta^{13}\text{C}$ values for ODP Hole 762C with
1225 depths (mbsf), adjusted depths (ambsf) and calibrated absolute ages (Ma).

1226

1227 Appendix 6: Age-depth plot for ODP Hole 762C. Horizontal axis shows standard
1228 tropical/subtropical planktonic foraminiferal and calcareous nannofossil biozones correlated
1229 to the Gradstein and others (2004) Geologic Time Scale. A line of correlation is drawn
1230 through each of the counted 100 kyr cycles below the K-Pg boundary (numbers 1 to 83). Nine

1231 average calculated sedimentation rates (cm/kyr) are shown for each significant change in
1232 slope of the line of correlation. Grey-shaded squares represent the uncertainties of magnetic
1233 polarity reversals.

1234

1235 Appendix 7: Exmouth Plateau age model based on Hole 762C versus a conventional age
1236 model based on Gradstein et al. (2004) and Huber et al. (2008) (Huber, B.T., MacLeod, K.G.,
1237 Tur, N.A., 2008. Chronostratigraphic framework for upper Campanian-Maastrichtian
1238 sediments on the Blake Nose (Subtropical North Atlantic). *J. Foraminiferal Res.* 38, 162–
1239 182). FO of *M. murus* at mid-latitudes (1) and low-latitudes (2) after Thibault et al. (2010).

1240 Thick grey lines of correlation indicate reliable biostratigraphic datums. Calcareous plankton
1241 diachronism is compelling.

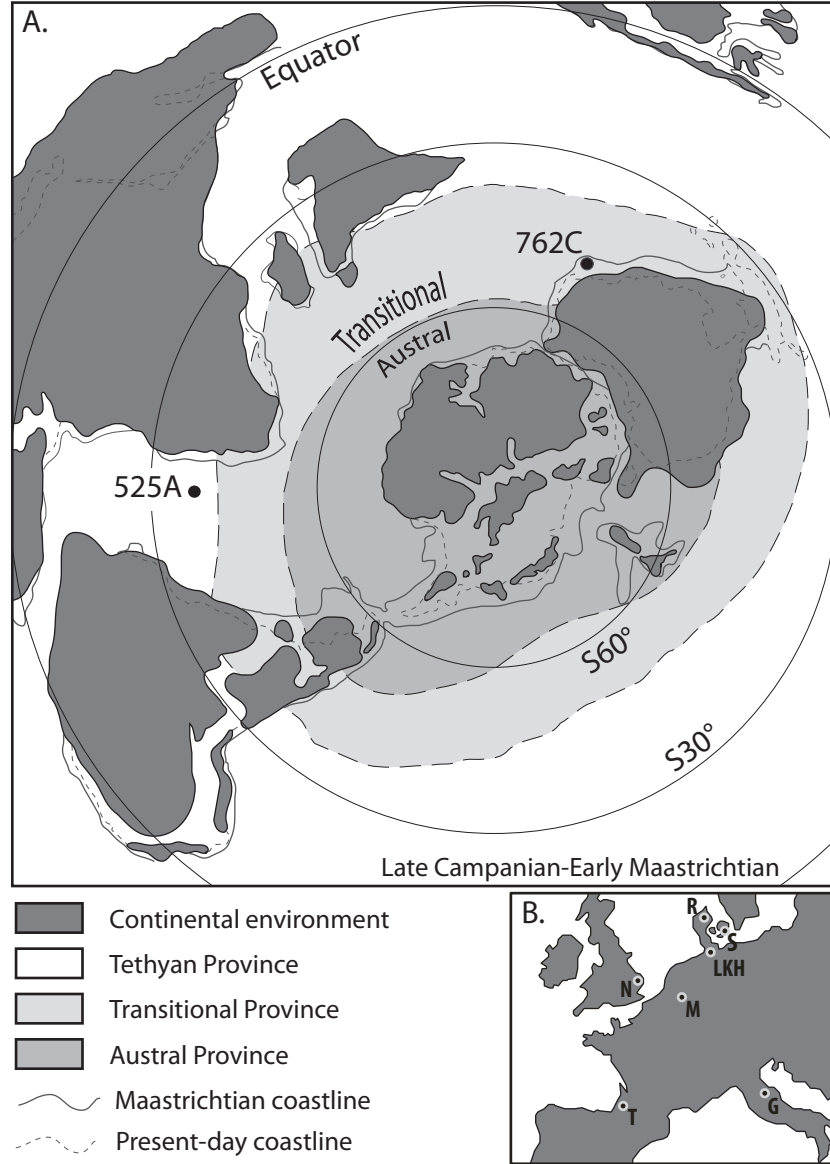


Figure 1 : A. Palaeogeographic reconstruction of the Southern Hemisphere for the upper Campanian-lower Maastrichtian showing the location of ODP Hole 762C, DSDP Hole 525A, and the inferred palaeobiogeographical boundaries between the Austral, Transitional and Tethyan provinces (from Huber, 1992a). B. Map of Europe showing other important locations of Campanian-Maastrichtian sections. G: Gubbio, LKH: Lägerdorf – Kronsmoor – Hemmoor, M: Maastricht, N: Norfolk, R: Rørdal, S: Stevns-1, T: Tercis les Bains.

Figure 2

[Click here to download high resolution image](#)

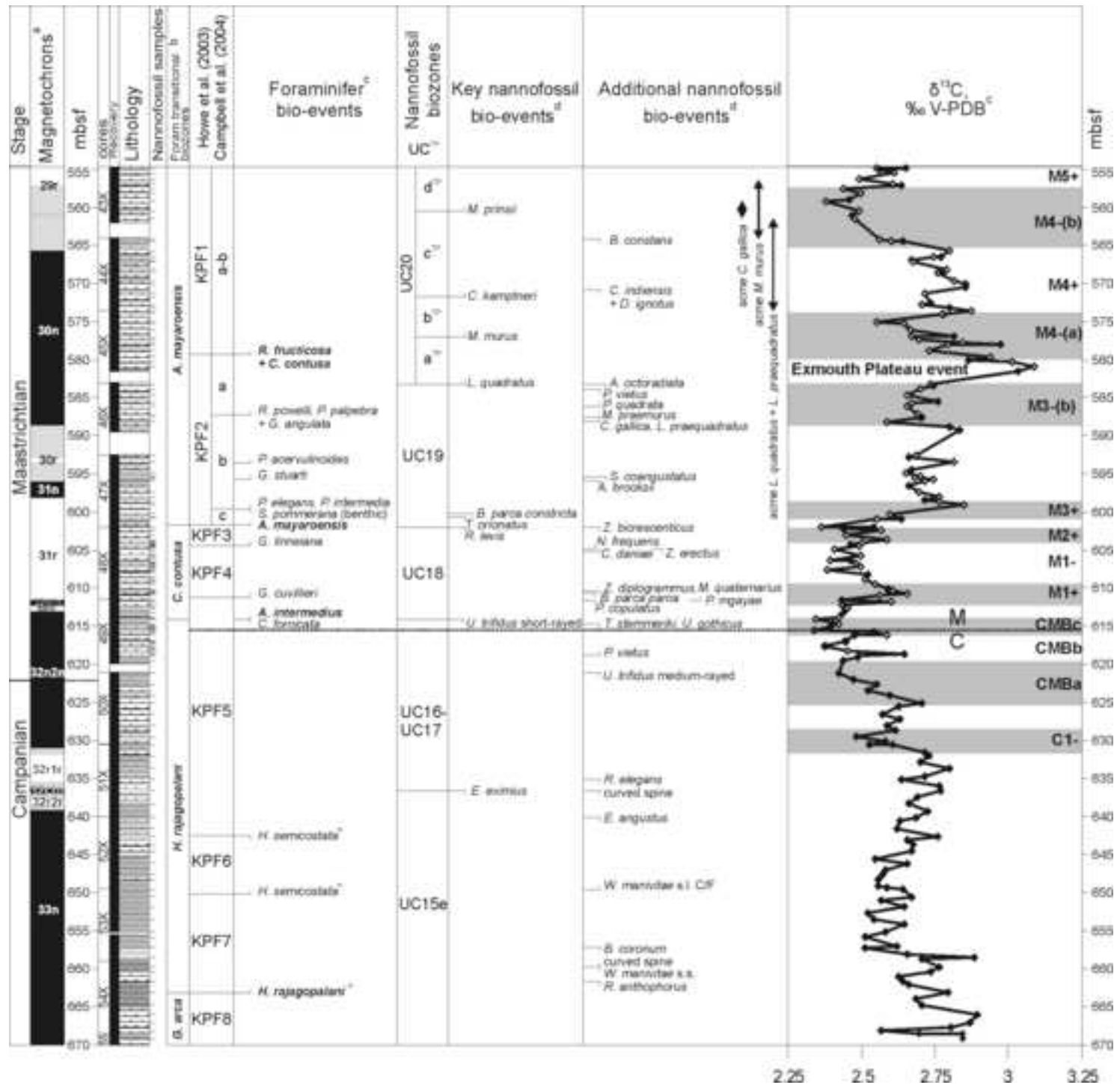


Figure4BW

[Click here to download high resolution image](#)

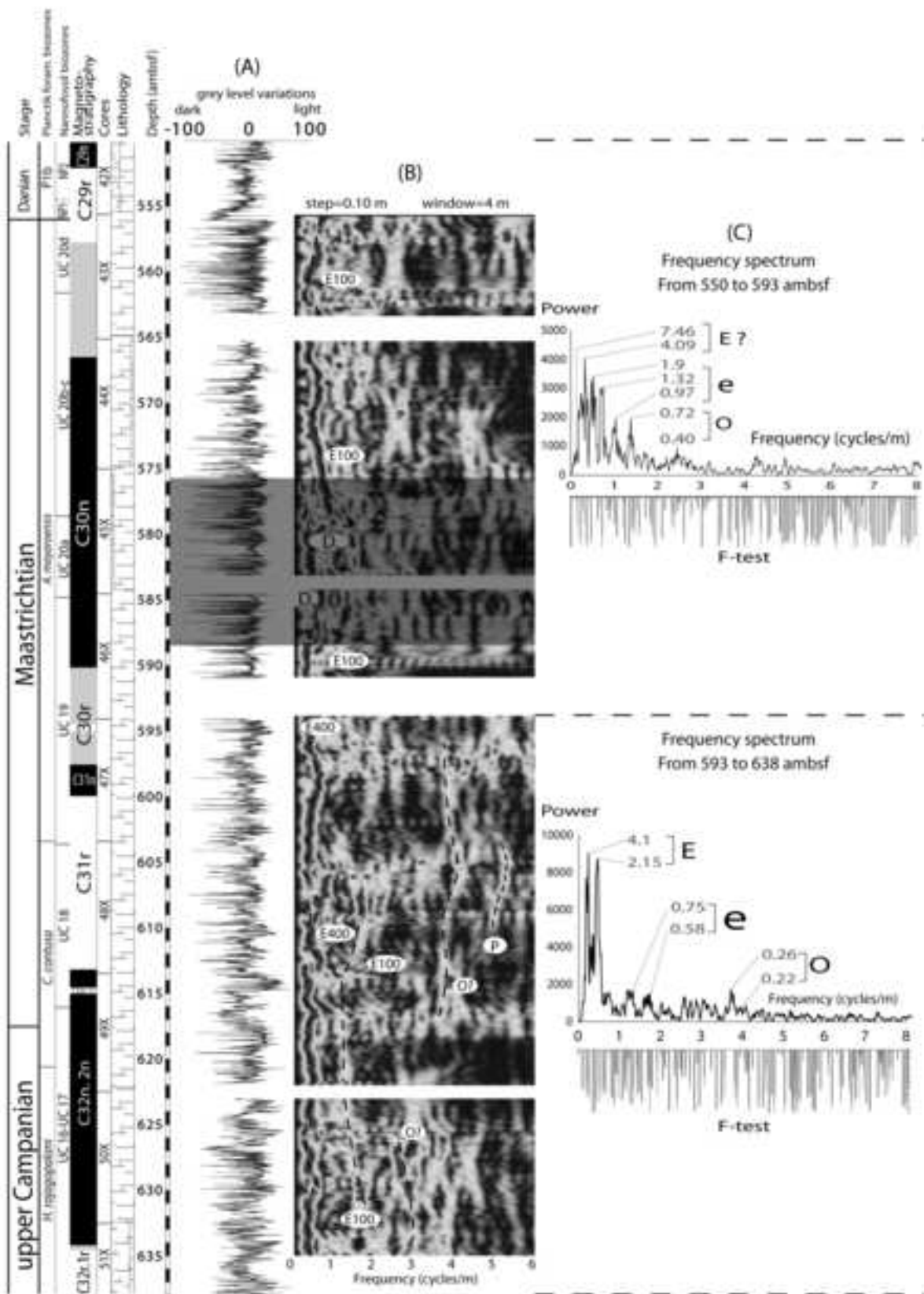


Figure 5
[Click here to download high resolution image](#)

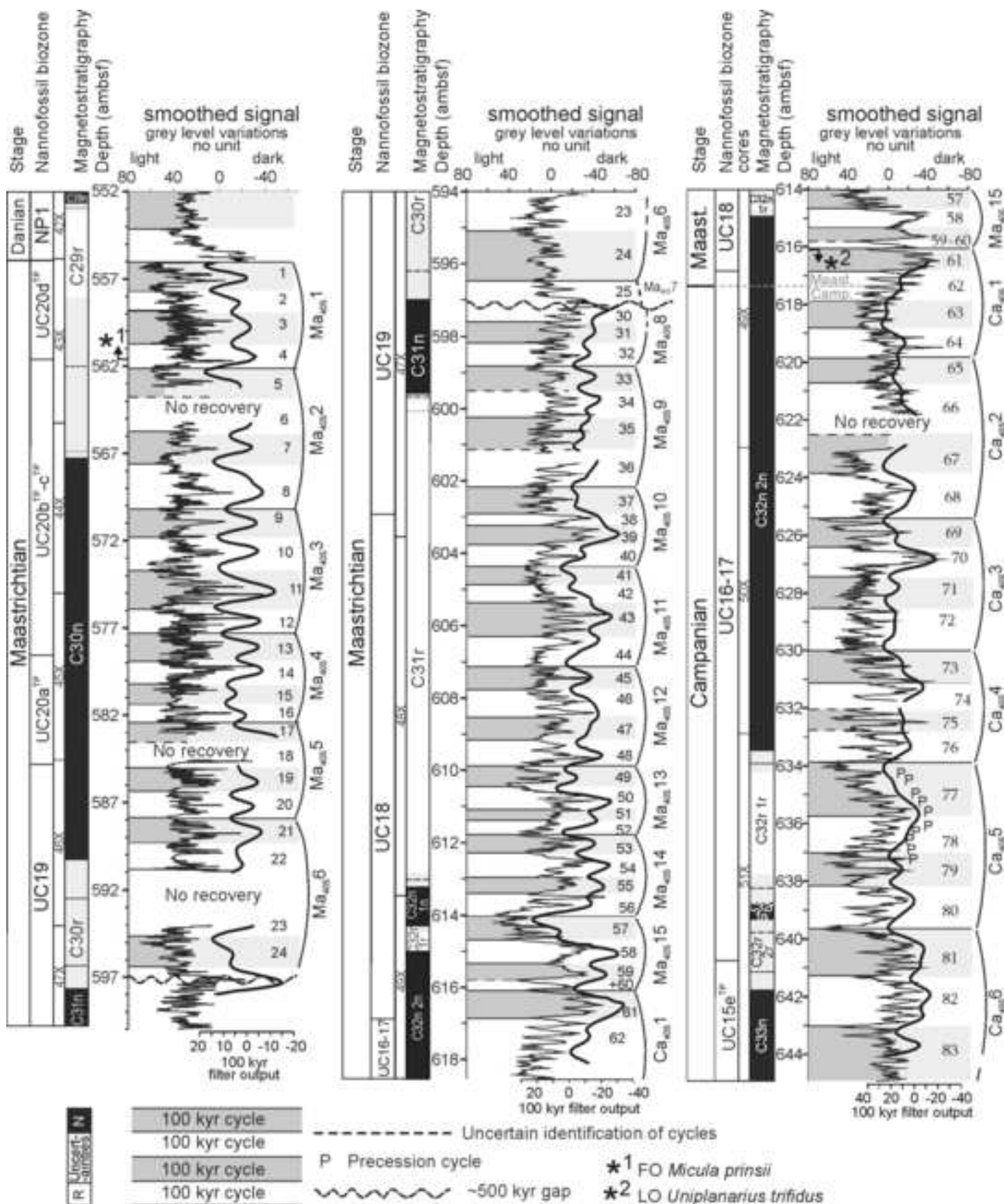


Figure6
[Click here to download high resolution image](#)

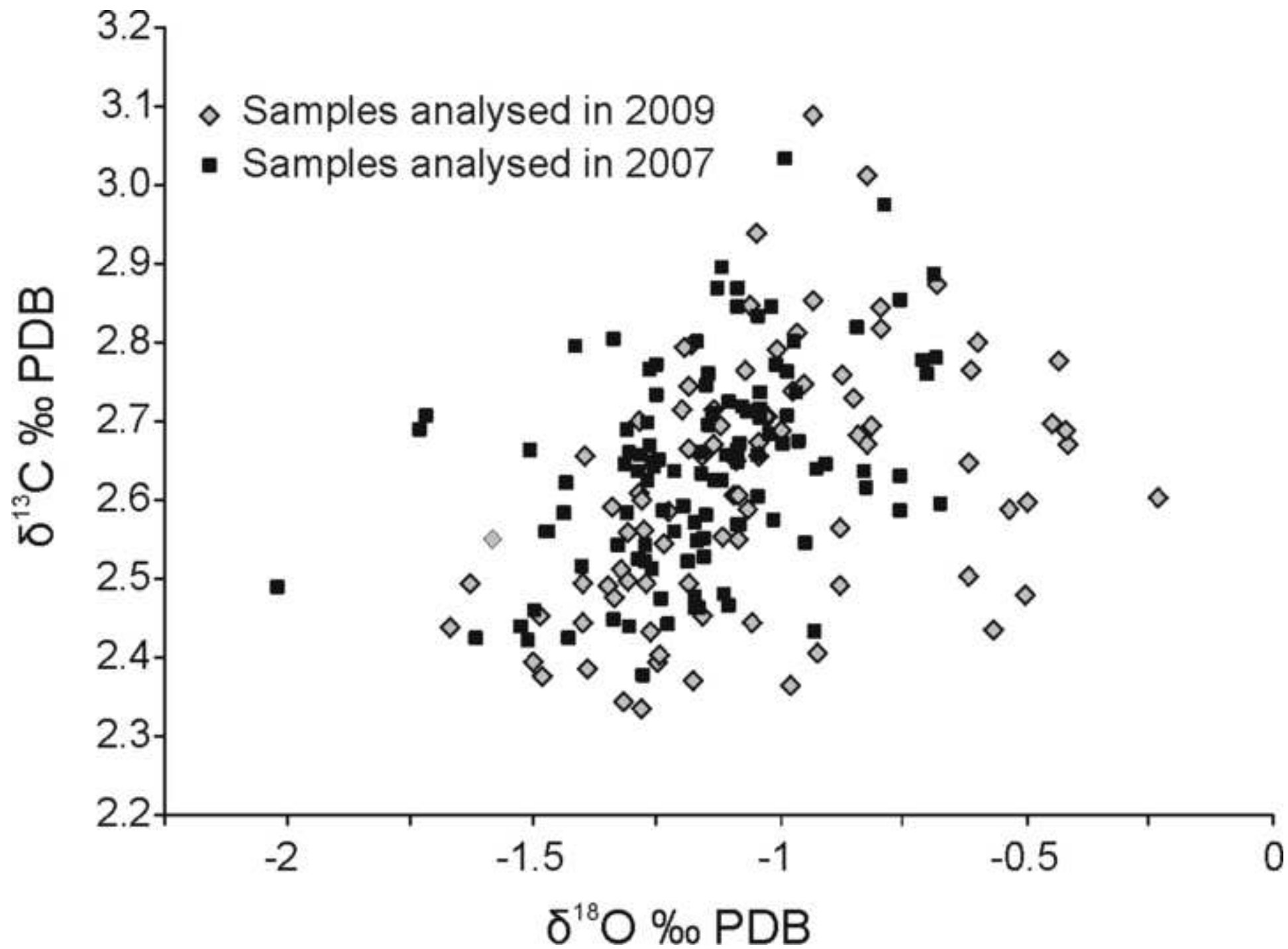


Figure 7

[Click here to download high resolution image](#)

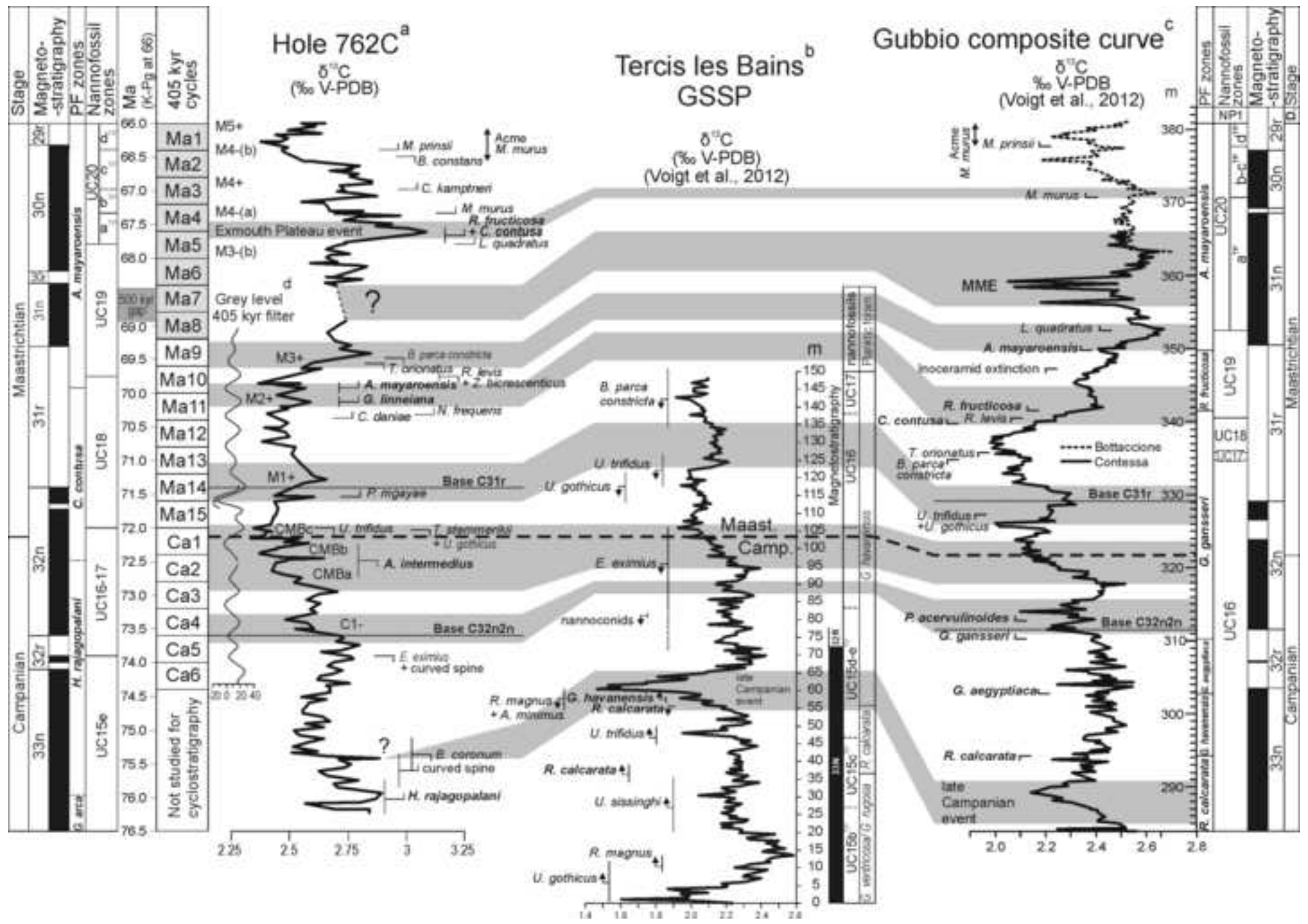


Figure 8
[Click here to download high resolution image](#)

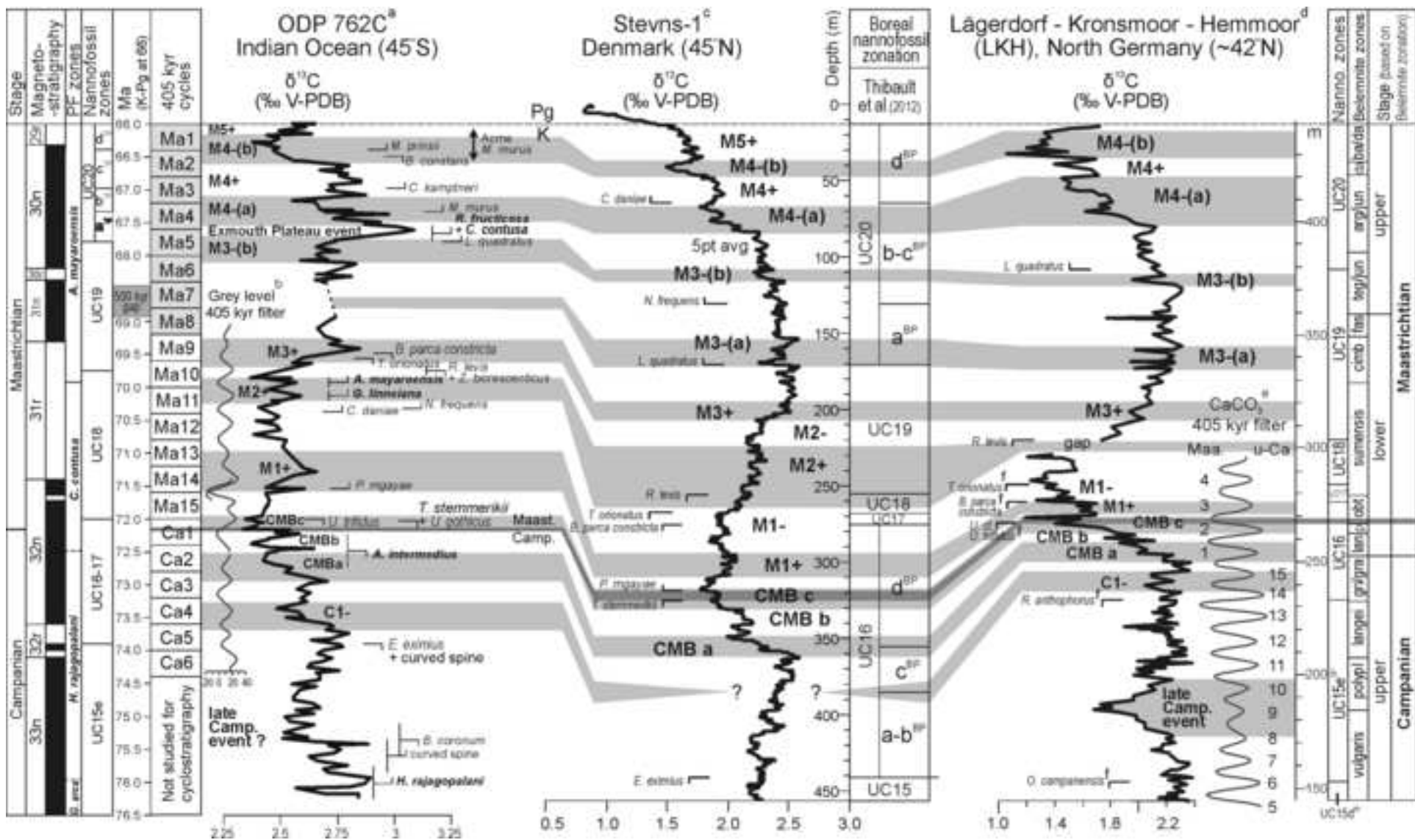


Figure 9
[Click here to download high resolution image](#)

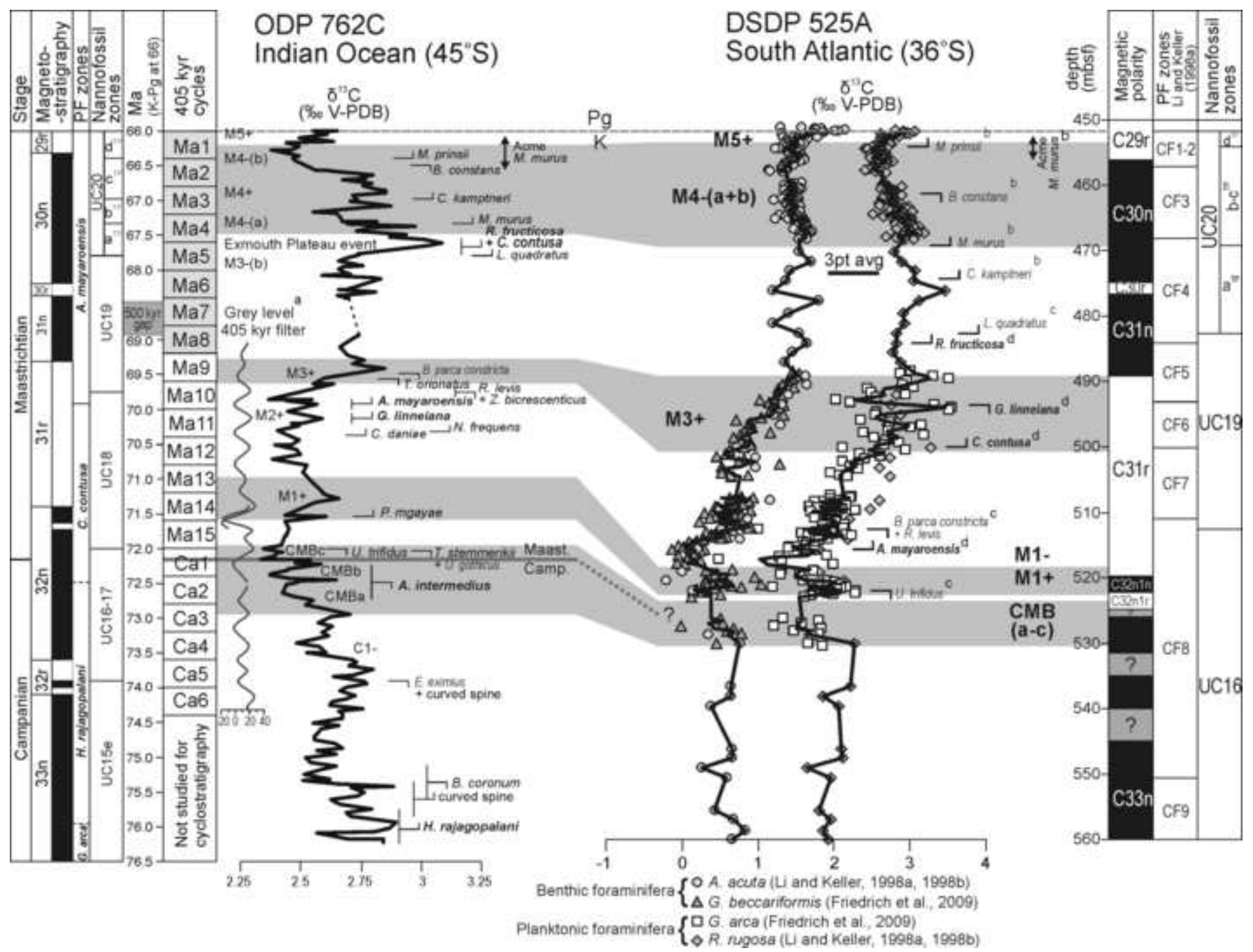
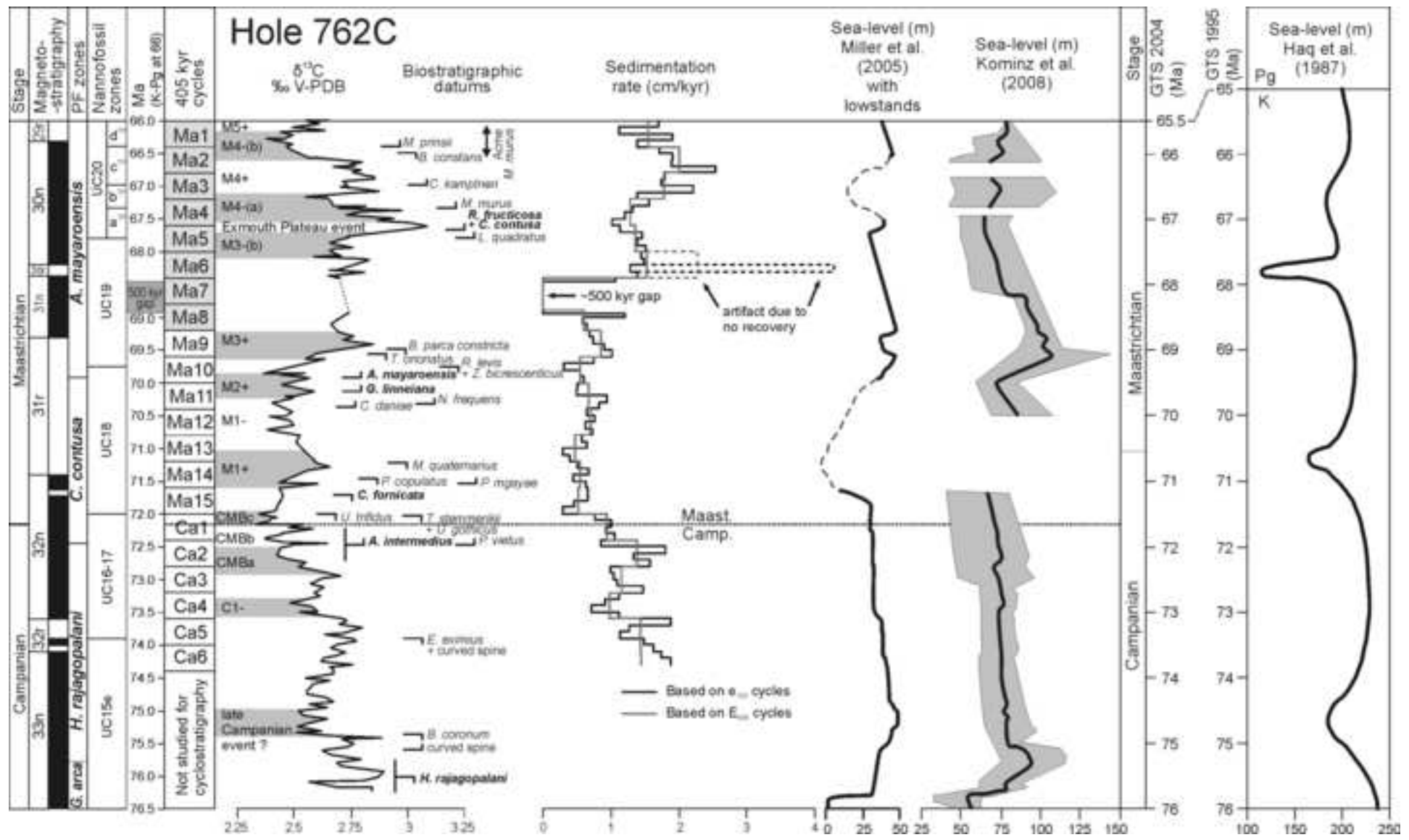
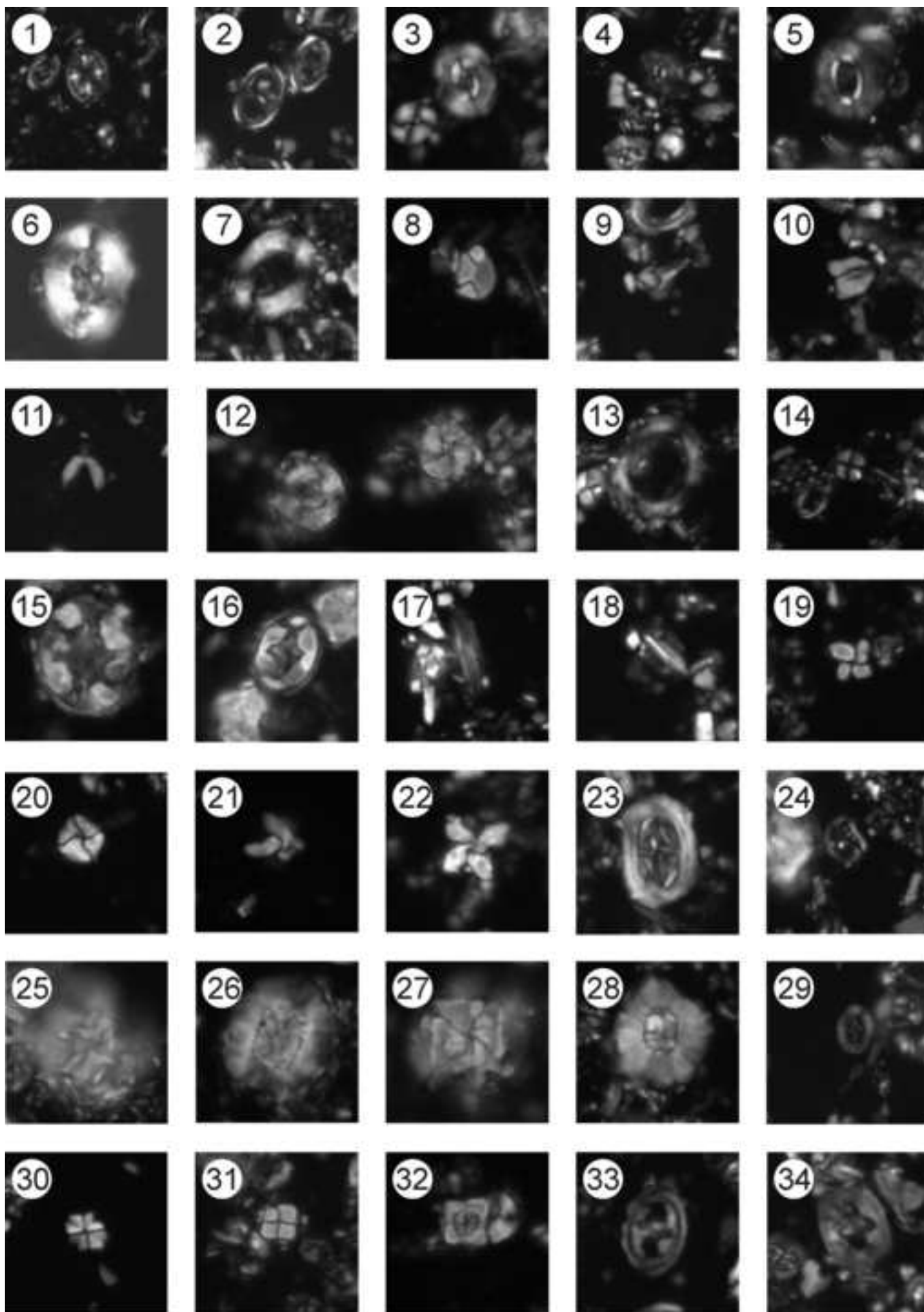
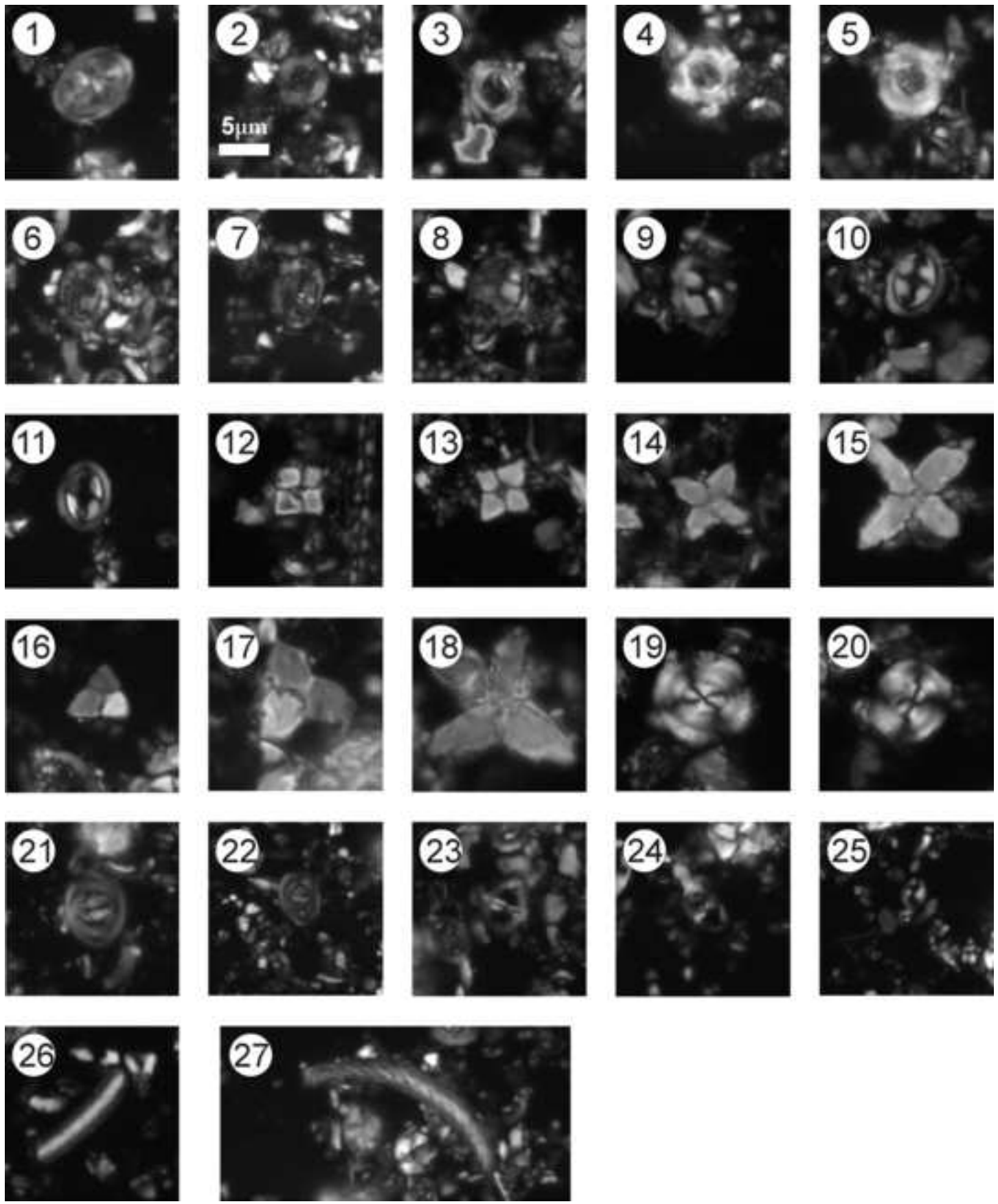


Figure 10
[Click here to download high resolution image](#)







Events	Top depth (mbsf)	Bottom depth (mbsf)	Top depth (amsf)	Bottom depth (amsf)	Age (Ma) with K/Pg at 66 Ma	Uncertainty (Ma)
K-Pg boundary	554.80	554.80	556.03	556.03	66.00	-
Top Acme <i>M. murus</i> ^a	555.51	556.33	556.74	557.56	66.07	±0.06
Top Acme <i>C. gallica</i> ^a	558.16	559.08	559.39	560.31	66.24	±0.07
FO <i>M. prinsii</i> ^a	560.46	561.40	561.69	562.63	66.39	±0.07
Base Acme <i>C. gallica</i> ^a	560.46	561.40	561.69	562.63	66.39	±0.06
Top Acme <i>L. quadratus</i> ^a & <i>L. praequadratus</i> ^a	560.46	561.40	561.69	562.63	66.39	±0.06
LO <i>B. constans</i> ^a	561.40	564.14	562.63	565.37	66.49	±0.1
Base Acme <i>M. murus</i> ^a	564.14	564.42	565.37	565.65	66.56	±0.04
LO <i>C. indiensis</i> ^a , <i>D. ignotus</i> ^a	569.60	570.80	570.83	572.03	66.87	±0.07
FO <i>C. kamptneri</i> ^a	571.70	572.78	572.93	574.01	66.98	±0.1
Base Acme <i>L. quadratus</i> ^a & <i>L. praequadratus</i> ^a	573.60	573.97	574.83	575.20	67.07	±0.05
FO <i>M. murus</i> ^a	576.99	577.83	578.54	579.38	67.33	±0.07
FO <i>R. fructicosa</i> ^b , <i>C. contusa</i> ^b	579.30	584.00	580.85	585.55	67.66	±0.22
FO <i>L. quadratus</i> ^a , LO <i>A. octoradiata</i> ^a	583.20	583.89	584.75	585.44	67.79	±0.06
LO <i>P. vietus</i> ^a	583.20	583.89	584.75	585.44	67.79	±0.06
FO <i>P. quadrata</i> ^a	586.10	587.21	587.65	588.76	68.02	±0.08
FO <i>P. palpebra</i> ^b , <i>G. angulata</i> ^b , <i>R. powelli</i> ^b	587.20	593.60	588.75	595.15	68.18	±0.18
FO <i>M. praemurus</i> ^a	587.55	588.15	589.10	589.70	68.07	±0.05
FO <i>L. praequadratus</i> ^a , <i>C. gallica</i> ^a	588.15	592.59	589.70	594.14	68.18	±0.13
FO <i>P. acervulinooides</i> ^b	593.60	595.70	595.15	597.25	68.36	±0.08
LO <i>S. coangustatus</i> ^a	595.28	595.40	596.83	596.95	68.40	±0.04
LO <i>A. brooksii</i> ^a	595.65	595.90	597.20	597.45	68.95	±0.06
FO <i>G. stuarti</i> ^b	595.70	599.60	597.25	601.15	69.30	±0.12
LO <i>B. parca constricta</i> ^a	599.09	600.23	600.64	601.78	69.48	±0.1
FO <i>P. elegans</i> ^b , <i>P. intermedia</i> ^b , LO <i>S. pommerana</i> ^c	599.60	600.60	601.15	602.15	69.54	±0.09
LO <i>T. orionatus</i> ^a	600.23	600.66	601.78	602.21	69.56	±0.07
LO <i>R. levis</i> ^a , <i>Z. bicrescenticus</i> ^a	600.83	602.04	602.44	603.65	69.75	±0.15
FO <i>A. mayaroensis</i> ^b	601.70	603.00	603.31	604.61	69.92	±0.15
LO <i>G. linneiana</i> ^b	603.00	604.40	604.61	606.01	70.13	±0.14
LO <i>Z. erectus</i> ^a	604.64	604.82	606.25	606.43	70.28	±0.05
FO <i>N. frequens</i> ^a	604.82	605.20	606.43	606.81	70.32	±0.06
FO <i>C. daniae</i> ^a	605.20	605.57	606.81	607.18	70.37	±0.06
LO <i>M. quaternarius</i> ^a , <i>Z. diplogrammus</i> ^a	610.18	610.37	611.79	611.98	71.22	±0.05
LO <i>B. parca parca</i> ^a	610.54	610.67	612.15	612.28	71.28	±0.05
LO <i>P. copulatus</i> ^a	610.97	611.59	612.94	613.56	71.46	±0.09
FO <i>P. mgayae</i> ^a	611.59	611.79	613.56	613.76	71.54	±0.05
FO <i>G. cuvillieri</i> ^d , LO <i>C. fornicata</i> ^d	611.20	614.10	613.17	616.07	71.71	±0.3
LO <i>U. trifidus</i> short-rayed ^a	614.00	614.12	615.97	616.09	72.00	±0.05
LO <i>T. stemmeriki</i> ^a , <i>U. gothicus</i> ^a	614.12	614.70	616.09	616.67	72.03	±0.07
Campanian-Maastrichtian boundary level	-	615.40	-	617.37	72.15	±0.05
FO <i>A. intermedius</i> ^d	614.10	624.00	616.07	625.97	72.48	±0.39
FO <i>P. vietus</i> ^a	618.82	618.85	620.79	620.82	72.47	±0.04
LO <i>U. trifidus</i> medium-rayed ^a	619.50	621.11	621.47	623.08	72.57	±0.09
LO <i>R. elegans</i> ^a	633.61	635.12	635.96	637.47	73.80	±0.06
LO <i>E. eximius</i> ^a , curved spine ^a	635.12	636.60	637.47	638.95	73.90	±0.09
LO <i>H. semicostata</i> ^d	637.10	642.50	639.45	645.12	74.20	±0.23
LO <i>E. angustus</i> ^a	638.36	640.11	640.71	642.46	74.15	±0.06
<i>W. manivitae</i> ^a s.l. C/F	648.35	649.63	650.97	652.25	74.83	±0.4
LO <i>B. coronum</i> ^a	655.91	657.19	658.53	659.81	75.36	±0.4
LO <i>W. manivitae</i> ^a s.s.	658.52	659.77	661.14	662.39	75.54	±0.4
FO curved spine ^a	659.77	660.39	662.39	663.01	75.60	±0.4
LO <i>R. anthophorus</i> ^a	660.39	661.72	663.01	664.34	75.67	±0.4
FO <i>H. rajagopalani</i> ^d	663.2	670.2	665.82	672.82	76.06	±0.4

Table 1

Table2

[Click here to download Table: Table2-magnetostratigraphy.xls](#)

Events	depth (mbsf)	ambsf	GTS2004	Husson et al. (2011)	
				Ref. Site	Option 2
K-Pg boundary	554.8	556.03	65.500	1267B	66±0.07
C29r/C30n	560.91+/-4.41	562.14	65.861	1267B	66.3±0.08
C30n/C30r	590.79 +/-2.15	592.34	67.696	1267B	68.2±0.08
C30r/C31n	594.72 +/-1.21	596.27	67.809	525A	68.32±0.07
C31n/C31r	598.16 +/-0.04	599.71	68.732	525A	69.22±0.07
C31r/C32n1n	611.46 +/-0.06	613.07	70.961	762C	71.4±0.08
C32n1n/C32n1r	612.37 +/-0.18	614.34	71.225	762C	71.64±0.07
C32n1r/C32n2n	612.975 +/-0.075	614.95	71.474	762C	71.72±0.07
C32n2n/C32r1r	631.475 +/-0.395	633.83	72.929	762C	73.6±0.08
C32r1r/C32r1n	635.885 +/-0.465	638.24	73.231	762C	73.9±0.09
C32r1n/C32r2r	637.39 +/-0.45	639.74	73.318	762C	74±0.08
C32r2r/C33n	638.78 +/-0.35	641.13	73.577	762C	74.1±0.08

Table 2a

Magnetochron	Duration in this study (Ma)	Husson et al. (2011)	GTS2004
C29r (Cretaceous)	0.397+/-0.22	0.3+/-0.02	0.361
C30n	1.798+/-0.16	1.9+/-0.03	1.835
C30r	0.173+/-0.07*	~0.12	0.113
C31n	-	~0.9	0.923
C31r	2.18+/-0.03	<i>id.</i>	2.229
C32n1n	0.240+/-0.06	<i>id.</i>	0.264
C32n1r	0.08+/- 0.03	<i>id.</i>	0.249
C32n2n	1.88 +/- 0.03	<i>id.</i>	1.456
C32r1r	0.3+/-0.06	<i>id.</i>	0.301
C32r1n	0.1+/-0.03	<i>id.</i>	0.087
C32r2r	0.1 +/- 0.04	<i>id.</i>	0.259

Table 2b

Table3

[Click here to download Table: Table3-description of 13C events.xls](#)

Carbon-isotope events	Stratigraphic interval	Top depth (mbsf)	Bottom depth (mbsf)	Description
M5+	upper Maastrichtian	554.80	557.36	Rapid 0.2‰ increase up to values around 2.6‰
M4-(b)	upper Maastrichtian	557.36	565.27	Sharp 0.4‰ negative decrease reaching a minimum value of 2.38‰
M4+	upper Maastrichtian	565.27	573.79	Positive 0.25‰ rebound with values fluctuating around 2.77‰
M4-(a)	upper Maastrichtian	573.79	579.93	Fluctuating values resulting in a progressive 0.55‰ decrease from 3.1 to 2.55‰
Exmouth Plateau event	upper Maastrichtian	579.93	583.20	Sharp 0.4‰ positive excursion up to values of 3.1‰
M3-(b)	upper Maastrichtian	583.20	588.75	Short-lived 0.1‰ negative excursion from values around 2.8 to values around 2.7‰
M3+	lower Maastrichtian	598.48	600.89	Rapid 0.3‰ increase up to 2.85‰
M2+	lower Maastrichtian	602.05	604.43	short-lived 0.1‰ positive excursion with values fluctuating around 2.55‰
M1-	lower Maastrichtian	604.43	609.45	Slight 0.1‰ negative excursion with values fluctuating gently around 2.45‰
M1+	lower Maastrichtian	609.45	612.11	Values increase from 2.45 to 2.7‰
CMB c	CMB	613.84	615.66	Third step of CMBE characterized by a 0.3‰ negative shift from 2.6 to 2.3‰
CMB b	upper Campanian	615.66	619.50	Second step of CMBE characterized by rapid fluctuations between 2.4 and 2.6‰
CMB a	upper Campanian	619.50	625.34	First step of CMBE characterized by a 0.3‰ negative shift from 2.7 to 2.4‰
C1-	upper Campanian	628.50	631.70	0.25‰ negative excursion from 2.75 to 2.5‰, immediately followed by a 0.15‰ positive rebound
late Campanian event ?	upper Campanian	650.80	658.05	long-lasting 0.2‰ negative excursion with values shifting from an average of 2.8‰ to c. 2.6‰

Table 3

Table4

[Click here to download Table: Table4-age of C13 events.xls](#)

Carbon isotope Events	Top depth (mbsf)	Base depth (mbsf)	Top depth (ambsf)	Base depth (ambsf)	Age (Ma), K-Pg at 66		Duration (Ma)
					Top	Base	
M5+	554.80	557.36	556.03	558.59	66.00	66.16	0.16
M4-(b)	557.36	565.27	558.59	566.50	66.16	66.60	0.44
M4+	565.27	573.79	566.50	575.34	66.60	67.11	0.51
M4-(a)	573.79	579.93	575.34	581.48	67.11	67.54	0.43
Exmouth Plateau event	579.93	583.20	581.48	584.75	67.54	67.77	0.23
M3-(b)	583.20	588.75	584.75	590.30	67.77	68.11	0.34
M3+	598.48	600.89	600.03	602.44	69.34	69.64	0.30
M2+	602.05	604.43	603.66	606.04	69.87	70.24	0.38
M1-	604.43	609.45	606.04	611.06	70.24	71.04	0.80
M1+	609.45	612.11	611.06	614.08	71.04	71.62	0.57
CMBc	613.84	615.66	615.81	617.63	71.94	72.16	0.22
CMBb	615.66	619.50	617.63	621.47	72.16	72.52	0.35
CMBa	619.50	625.34	621.47	627.31	72.52	72.95	0.43
C1-	628.50	631.70	630.47	633.67	73.28	73.57	0.29
late Campanian event ?	650.80	658.05	653.42	660.67	74.96	75.40	0.44

Table 4

Samples	Depth mbsf	Inclination (°)	Chron	Paleomagnetic Interpretation	Remarks	ambsf
ODP Leg 122 Hole 762C						
42X4, 80	550.3	-58		C29n		
42X5, 75	551.76	-2		?		
42X5, 130	552.3	11				
42X6, 25	552.75	6				
42X6, 136	553.86	29		C29r		
43X1, 41	554.91	41			K-Pg at 554.8 mbsf	
43X1, 100	555.5	53				
43X2, 50	556.5	20	C29r base of Galbrun (1992) does not fit with the FO of <i>M. prinsii</i>			557.73
43X2, 110	557.1	-40 weak				558.33
43X3, 42	557.92	-55 ?				
43X3, 141	558.91	-18 weak				
43X4, 20	559.2	-12 weak				
43X4, 113	560.13	-22 weak		?		
43X5, 22	560.72	3 weak			FO <i>Micula prinsii</i> at 560.46 mbsf	
43X5, 96	561.46	-23 weak				
44X1, 51	564.51	-59 ?				
44X1, 132	565.32	52	C29r larger uncertainty			566.55
44X2, 52	566.02	-56	C30n			567.25
44X2, 132	566.83	-76				
44X3, 126	568.26	-46				
44X4, 95	569.45	-49				
44X5, 102	571.02	-62				
44X6, 67	572.17	-44				
45X1, 29	573.79	-61				
45X2, 112	576.12	-58				
45X3, 86	577.36	-65				
45X4, 60	578.6	-23		C30n		
45X4, 111	579.11	-32				
45X5, 24	579.74	-13				
45X5, 110	580.6	-64				
46X1, 44	583.44	-61				
46X1, 120	584.2	-9				
46X2, 41	584.91	34				
46X2, 117	585.67	-42				
46X3, 45	586.45	-44				
46X3, 117	587.17	-52				
46X4, 38	587.88	-49				
46X4, 114	588.64	-57	C30n		No recovery interval between 589.5 and 592.5 mbsf	590.19
47X1, 44	592.94	55	C30r	C30r		594.49
47X2, 101	593.51	18	C30r			595.06
47X3, 43	595.93	-16	C31n		~500 kyr gap around 595.45 mbsf	597.48
47X3, 95	596.45	-73				
47X4, 48	597.48	-34		C31n		
47X4, 89,5	597.89	-48				
47X4, 112	598.12	-62	C31n			599.67
47X4, 120	598.2	57	C31r			599.75
47X4, 140	598.4	75				
47X5, 4	598.54	48				
47X5, 19	598.69	52				
47X5, 32	598.82	70				
47X5, 39,5	598.89	64				
47X5, 46	598.96	75				
47X5, 101	599.51	63				
47X6, 40	600.4	83		C31r		
48X1, 54	602.54	80				
48X2, 36	603.86	58				
48X3, 30	605.3	67				
48X4, 65	607.15	67				
48X5, 131	609.31	63				
48X6, 47	609.97	63				
48X7, 30	611.31	66				
48XCC, 6	611.4	57	C31r			613.01
48XCC, 18	611.52	-42	C32n1n			613.13
49X1, 10	611.6	-25				

49X1, 26,5	611.76	-14		
49X1, 37	611.87	-45		
49X1, 48	611.98	-24		
49X1, 58	612.08	-40		
49X1, 78	612.28	-48	C32n1n	614.25
49X1, 96	612.46	31	C32n1r	614.43
49X1, 118	612.68	52		
49X1, 122	612.72	56		
49X1, 142,5	612.92	56	C32n1r	614.89
49X2, 3,5	613.03	-70	C32n2n	615
49X2, 20,5	613.2	-45		
49X2, 49,5	613.42	-55		
49X2, 45	613.45	-51		
49X2, 117	614.17	-40		
49X3, 46	614.96	53		very small reverse within C32n2n ?
49X3, 109	615.59	-54		
49X4, 50	616.5	-49		
49X4, 111	617.11	-59		
49X5, 41	617.91	-63		
49X5, 108	618.58	-59		
50X1, 47	621.47	-15		
40X1, 113	622.14	-44		
50X2, 102	623.52	-58		
50X3, 98	624.98	-55		
50X4, 104	626.54	-59		
50X5, 47	627.47	-56		
50X6, 121	629.71	-66		
50X7, 37	630.38	-69		
51X1, 58	631.08	-46	C32n2n	633.43
51X1, 135	631.87	38	C32r1r	634.22
51X2, 141	633.41	41		
51X3, 117	634.67	68		
51X4, 42	635.42	70	C32r1r	637.77
51X4, 135	636.35	-30	C32r1n	638.7
51X5, 44	636.94	-23	C32r1n	639.29
51X5, 133	637.84	8	C32r2r	640.19
51X6, 43	638.43	8	C32r2r	640.78
51X6, 112	639.13	-32	C33n	641.48
52X1, 117	641.17	-75		
52X2, 122	642.72	-54		
52X3, 114	644.14	-54		
52X4, 141	645.91	-71		

...and so on until 704.72 mbsf for base C33n

In black, samples from Galbrun (1992)

In bold grey, additional samples analysed by Galbrun in 2008

Appendix 1

Appendix 2: Alphabetical list of calcareous nannofossil species. All references prior to 1998 can be found in Perch-Nielsen (1985) and Bown (1998). Others are given in the reference list below.

Ahmuellerella octoradiata (Gorkà, 1957) Reinhardt, 1966

Amphizygus brooksii Bukry, 1969

Biscutum constans (Gorkà, 1957) Black *in* Black and Barnes, 1959

Biscutum coronum Wind and Wise *in* Wise and Wind, 1977

Biscutum magnum Wind and Wise *in* Wise and Wind, 1977

Broinsonia parca constricta Hattner et al., 1980

Broinsonia parca parca Hattner et al., 1980

Calculites obscurus (Deflandre, 1959) Prins and Sissingh *in* Sissingh, 1977

Ceratolithoides aculeus (Stradner, 1961) Prins and Sissingh *in* Sissingh, 1977

Ceratolithoides indiensis Burnett, 1997a

Ceratolithoides kamptneri Bramlette and Martini, 1964

Cribrocorona gallica (Stradner, 1963) Perch-Nielsen, 1973

Cribrospheraella daniae Perch-Nielsen, 1973

Discorhabdus ignotus (Gorkà, 1957) Perch-Nielsen, 1968

Eiffellithus angustus (Bukry, 1969) Shamrock and Watkins, 2009

Eiffellithus eximius (Stover, 1966) Perch-Nielsen, 1968

Lithraphidites praequadratus Roth, 1978

Lithraphidites quadratus Bramlette and Martini, 1964

Micula murus (Martini, 1961) Bukry, 1973

Micula praemurus (Bukry, 1973) Stradner and Steinmetz, 1984

Micula prinsii Perch-Nielsen, 1979

Monomarginatus quaternarius Wind and Wise *in* Wise and Wind, 1977

Nephrolithus frequens Gorkà, 1957

Petrarhabdus copulatus (Deflandre, 1959) Wind and Wise *in* Wise, 1983

Petrarhabdus vietus Burnett, 1997b

Prediscosphaera mgayae Lees, 2007

Pseudomicula quadrata Perch-Nielsen *in* Perch-Nielsen et al., 1978

Quadrum gartneri Prins and Perch-Nielsen *in* Manivit et al., 1977

Quadrum svabenickae Burnett, 1997b

Reinhardtites anthophorus (Deflandre, 1959) Perch-Nielsen, 1968

Reinhardtites elegans (Gartner, 1968) Wise, 1983

Reinhardtites levis Prins and Sissingh *in* Sissingh, 1977

Rotelapillus laffittei (Noël, 1956) Howe, Bergen and Campbell *in* Howe et al., 2003

Stoverius achylosus (Stover, 1966) Perch-Nielsen, 1986

Stoverius coangustatus Howe, Bergen and Campbell *in* Howe et al., 2003

Tortolithus hallii (Bukry, 1969) Crux *in* Crux et al., 1982

Tranolithus orionatus (Reinhardt, 1966a) Reinhardt, 1966b

Tranolithus stemmerikii Thibault and Sheldon *in* Thibault, 2010

Uniplanarius gothicus (Deflandre, 1959) Prins and Perch-Nielsen *in* Manivit et al., 1977

Uniplanarius trifidus (Stradner *in* Stradner and Papp, 1961) Hattner and Wise, 1980

Watznaueria manivittiae Bukry, 1973

Zeugrhabdotus bicrescenticus (Stover, 1966) Burnett *in* Gale et al., 1996

Zeugrhabdotus diplogrammus (Deflandre *in* Deflandre and Fert, 1954) Burnett *in* Gale et al., 1996

Zeugrhabdotus erectus (Deflandre *in* Deflandre and Fert, 1954) Reinhardt, 1965

References

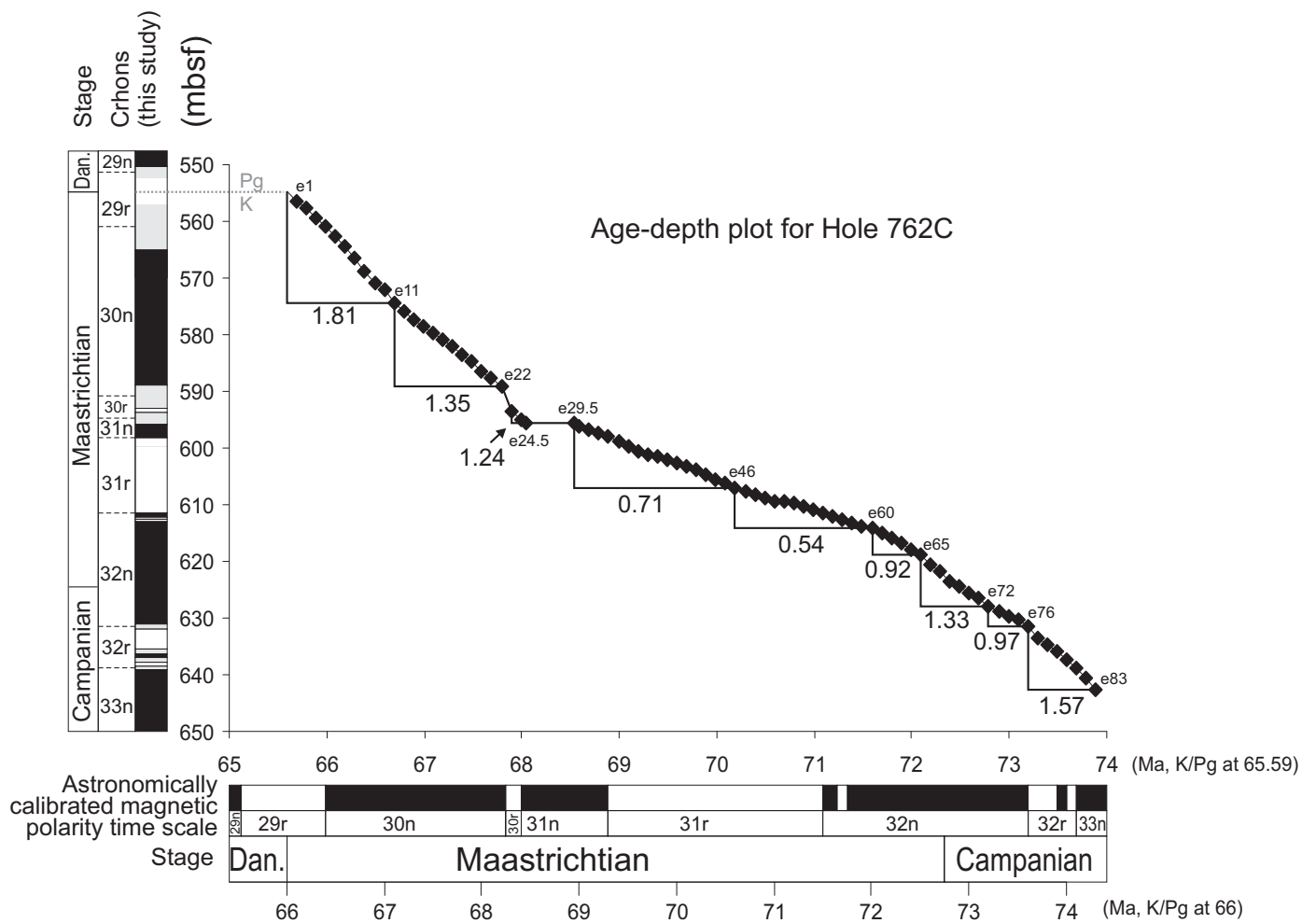
- Burnett, J.A., 1997a. New species and conjectured evolutionary trends of *Ceratholithoides* Bramlette and Martini, 1964 from the Campanian and Maastrichtian of the Indian Ocean. *Journal of Nannoplankton Research* 19, 123–131.
- Burnett, J.A., 1997b. New species and new combinations of Cretaceous nannofossils, and a note on the origin of *Petrarhabdus* (Deflandre) Wind and Wise. *Journal of Nannoplankton Research* 19, 133–146.
- Howe, R.W., Campbell, R.J., Rexilius, J.P., 2003. Integrated uppermost Campanian–Maastrichtian calcareous nannofossil and foraminiferal biostratigraphic zonation of the northwestern margin of Australia. *Journal of Micropalaeontology* 22, 29–62.
- Lees, J.A., 2007. New and rarely reported calcareous nannofossils from the Late Cretaceous of coastal Tanzania: outcrop samples and Tanzania Drilling Project Sites 5, 9 and 15. *Journal of Nannoplankton Research* 29, 39–65.
- Thibault, N., 2010. Calcareous nannofossils from the boreal Upper Campanian – Maastrichtian chalk of Denmark. *Journal of Nannoplankton Research* 31, 39–56.

Leg 122, Hole 762C, core, section, interval (cm)	Samples numbers	depth (mbsf)	adjusted depth (ambsf)	¹³ C standardized (‰ V-PDB)	Age (Ma) based on K/Pg at 65.59	Age (Ma) based on K/Pg at 66	100 kyr cycles
42X-5, 95-96	post-doc-1	551.95	552.98	1.40			
42X-CC, 35.5-35.5	post-doc-2	554.50	555.73	1.43			
43X-1, 33-34	PhD-129	554.83	556.06	2.55	65.592	66.002	e1
43X-1, 34-35	post-doc-3	554.85	556.08	2.65	65.593	66.003	
43X-1, 50-52	post-doc-4	555.01	556.24	2.56	65.602	66.012	
43X-1, 101-102	PhD-128	555.51	556.74	2.61	65.632	66.042	
43X-2, 33-34	PhD-127	556.33	557.56	2.49	65.680	66.090	
43X-2, 83-84	PhD-126	556.83	558.06	2.61	65.720	66.130	e2
43X-2, 103-104	post-doc-5	557.04	558.27	2.64	65.739	66.149	
43X-3, 4-5	PhD-125	557.54	558.77	2.44	65.784	66.194	
43X-3, 66-67	PhD-124	558.16	559.39	2.50	65.819	66.229	e3
43X-3, 147-148	post-doc-6	558.98	560.21	2.46	65.862	66.272	
43X-4, 8-9	PhD-123	559.08	560.31	2.38	65.867	66.277	
43X-4, 145-146	PhD-122	560.46	561.69	2.49	65.958	66.368	e4
43X-5, 47-48	post-doc-7	560.98	562.21	2.47	65.995	66.405	e5
43X-5, 90-91	PhD-121	561.40	562.63	2.48	66.019	66.429	
44X-1, 14-15	PhD-120	564.14	565.37	2.56	66.170	66.580	e6
44X-1, 42-43	PhD-119	564.42	565.65	2.60	66.185	66.595	
44X1-47-48	post-doc-8	564.48	565.71	2.64	66.188	66.598	
44X-2, 25-26	PhD-118	565.75	566.98	2.80	66.255	66.665	e7
44X-2, 95-96	PhD-117	566.45	567.68	2.75	66.292	66.702	e8
44X-2, 98-99	post-doc-9	566.48	567.71	2.77	66.293	66.703	
44X-2, 148-149	PhD-116	566.98	568.21	2.67	66.313	66.723	
44X-3, 9-10	PhD-115	567.09	568.32	2.68	66.317	66.727	
44X-3, 108-109	PhD-114	568.08	569.31	2.79	66.356	66.766	
44X-3, 147-148	post-doc-10	568.48	569.71	2.78	66.372	66.782	
44X-4, 5-6	PhD-113	568.55	569.78	2.76	66.368	66.778	e9
44X-4, 110-111	PhD-112	569.60	570.83	2.82	66.426	66.836	
44X-5, 8-9	PhD-111	570.08	571.31	2.85	66.453	66.863	
44X-5, 45-46	post-doc-11	570.45	571.68	2.85	66.474	66.884	
44X-5, 119-120	PhD-110	571.19	572.42	2.72	66.522	66.932	e10
44X-6, 95-96	post-doc-12	572.45	573.68	2.74	66.603	67.013	e11
44X-6, 128-129	PhD-108	572.78	574.01	2.71	66.618	67.028	
44X-7, 14-15	PhD-107	573.14	574.37	2.80	66.634	67.044	
45X-1, 10-11	PhD-106	573.60	575.15	2.87	66.655	67.065	
45X-1, 47-48	PhD-105	573.97	575.52	2.78	66.672	67.082	
45X-1, 50-51	post-doc-13	574.00	575.55	2.78	66.673	67.083	
45X-1, 145-146	PhD-104	574.95	576.50	2.55	66.732	67.142	e12
45X-2, 25-26	PhD-103	575.25	576.80	2.65	66.754	67.164	
45X-2, 113-114	PhD-102	576.13	577.68	2.66	66.814	67.224	e13
45X-3, 49-50	PhD-101	576.99	578.54	2.67	66.869	67.279	
45X-2, 100-102	post-doc-14	577.01	578.56	2.82	66.870	67.280	
45X-3, 88-89	PhD-100	577.38	578.93	2.69	66.895	67.305	e14
45X-3, 131-132	PhD-99	577.81	579.36	2.84	66.927	67.337	
45X-3, 149-150	post-doc-15	577.99	579.54	2.97	66.941	67.351	
45X-4, 5-6	PhD-98	578.05	579.60	2.80	66.946	67.356	
45X-4, 74-75	PhD-97	578.74	580.29	2.73	66.999	67.409	e15
45X-5, 4-5	PhD-96	579.54	581.09	2.94	67.065	67.475	
45X-5, 44-45	post-doc-16	579.95	581.50	2.87	67.101	67.511	e16
45X-5, 80-81	PhD-95	580.30	581.85	3.01	67.136	67.546	
45X-5, 143-144	PhD-94	580.93	582.48	3.09	67.197	67.607	e17
45X-CC, 40-42	post-doc-17	581.41	582.96	3.03	67.239	67.649	
46X-1, 20-21	PhD-93	583.20	584.75	2.74	67.373	67.783	e18
46X-1, 45-46	post-doc-18	583.45	585.00	2.74	67.391	67.801	e19
46X-1, 89-90	PhD-92	583.89	585.44	2.70	67.422	67.832	
46X-2, 8-9	PhD-91	584.58	586.13	2.66	67.472	67.882	
46X-2, 99-100	post-doc-19	585.50	587.05	2.76	67.535	67.945	e20
46X-2, 109-110	PhD-90	585.59	587.14	2.67	67.541	67.951	
46X-3, 10-11	PhD-89	586.10	587.65	2.66	67.575	67.985	
46X-3, 121-122	PhD-88	587.21	588.76	2.69	67.651	68.061	e21
46X-3, 147-148	post-doc-20	587.48	589.03	2.70	67.670	68.080	
46X-4, 5-6	PhD-87	587.55	589.10	2.71	67.674	68.084	

46X-4, 65-66	PhD-86	588.15	589.70	2.59	67.715	68.125 e22
46X-4, 125-126	post-doc-21	588.75	590.30	2.80	67.756	68.166
46X-CC, 33-34	post-doc-22	589.30	590.85	2.83	67.791	68.201 e23
47X-1, 9-10	PhD-85	592.59	594.14	2.69	67.868	68.278
47X-1, 23-24	post-doc-23	592.74	594.29	2.66	67.871	68.281
47X-1, 95-96	PhD-84	593.35	594.90	2.81	67.886	68.296
47X-2, 46-47	post-doc-24	594.46	596.01	2.67	67.957	68.367 e24
47X-2, 81-82	PhD-83	594.81	596.36	2.65	67.982	68.392
47X-2, 128-129	PhD-82	595.28	596.83	2.70	68.024	68.434 e24,5
47X-2, 140-141	PhD-81	595.40	596.95	2.68	68.489	68.899 e29,5
47X-3, 16-17	PhD-80	595.65	597.20	2.74	68.557	68.967 e30
47X-3, 40-41	PhD-79	595.90	597.45	2.71	68.577	68.987
47X-3, 111-112	post-doc-25	596.62	598.17	2.66	68.688	69.098 e31
47X-4, 40-41	PhD-78	597.40	598.95	2.69	68.808	69.218 e33
47X-4, 106-107	PhD-77	598.06	599.61	2.77	68.904	69.314 e34
47X-4, 147-148	post-doc-26	598.48	600.03	2.72	68.962	69.372
47X-5, 23-24	PhD-76	598.73	600.28	2.77	68.995	69.405 e35
47X-5, 59-60	PhD-75	599.09	600.64	2.85	69.035	69.445
47X-6, 23-24	PhD-74	600.23	601.78	2.60	69.157	69.567 e36
47X-6, 85-86	PhD-72	600.83	602.38	2.55	69.227	69.637 e37
47X-6, 88-89	post-doc-27	600.89	602.44	2.63	69.235	69.645
48X-1, 4-5	PhD-71	602.04	603.65	2.37	69.469	69.879 e39
47X-CC, 28-29	post-doc-28	602.05	603.66	2.54	69.471	69.881
48X-1, 10-11	post-doc-29	602.11	603.72	2.44	69.482	69.892
48X-1, 40-41	PhD-70	602.40	604.01	2.57	69.531	69.941 e40
48X-1, 100-101	PhD-69	603.00	604.61	2.45	69.640	70.050 e41
48X-2, 19-20	PhD-68	603.69	605.30	2.59	69.778	70.188 e42
48X-2, 60-61	PhD-65	604.11	605.72	2.50	69.828	70.238 e43
48X-2, 69-70	post-doc-30	604.20	605.81	2.46	69.838	70.248
48X-2, 93-94	PhD-62	604.43	606.04	2.49	69.862	70.272
48X-2, 132-133	PhD-59	604.82	606.43	2.41	69.906	70.316 e44
48X-3, 74-75	PhD-56	605.74	607.35	2.50	70.024	70.434 e45
48X-3, 125-126	post-doc-31	606.26	607.87	2.46	70.103	70.513 e46
48X-3, 129-130	PhD-54	606.29	607.90	2.39	70.107	70.517
48X-4, 30-31	PhD-51	606.80	608.41	2.48	70.173	70.583
48X-4, 73-74	PhD-48	607.23	608.84	2.50	70.239	70.649 e47
48X-4, 120-121	PhD-45	607.70	609.31	2.38	70.311	70.721 e48
48X-5, 26-27	post-doc-32	608.27	609.88	2.52	70.391	70.801 e49
48X-5, 78-79	PhD-42	608.78	610.39	2.51	70.481	70.891
48X-5, 145-146	PhD-39	609.45	611.06	2.54	70.586	70.996 e50
48X-6, 68-69	PhD-38	610.18	611.79	2.59	70.863	71.273 e53
48X-6, 71-72	post-doc-33	610.22	611.83	2.59	70.871	71.281
48X-6, 87-88	PhD-37	610.37	611.98	2.61	70.898	71.308 e54
48X-6, 117-118	PhD-34	610.67	612.28	2.66	70.943	71.353
48X-6, 147-148	PhD-33	610.97	612.58	2.56	70.988	71.398
49X-1, 10-12	post-doc-34	611.62	613.59	2.43	71.120	71.530 e56
49X-1, 23-24	PhD-30	611.75	613.72	2.60	71.141	71.551
49X-1, 61-62	PhD-29	612.11	614.08	2.43	71.197	71.607 e57
49X-1, 116-117	PhD-27	612.66	614.63	2.45	71.281	71.691
49X-2, 11-12	post-doc-35	613.12	615.09	2.44	71.351	71.761 e58
49X-2, 20-21	PhD-26	613.20	615.17	2.44	71.364	71.774
49X-2, 82-84	post-doc-36	613.84	615.81	2.42	71.493	71.903 e60
49X-2, 112-113	PhD-23	614.12	616.09	2.34	71.587	71.997
49X-3, 10-11	post-doc-37	614.61	616.58	2.42	71.653	72.063 e61
49X-3, 20-21	PhD-22	614.70	616.67	2.40	71.665	72.075
49X-3, 65-66	PhD-19	615.15	617.12	2.39	71.716	72.126 e62
49X-3, 104-105	PhD-16	615.55	617.52	2.34	71.756	72.166
49X-3, 115-116	post-doc-38	615.66	617.63	2.54	71.767	72.177
49X-4, 11-12	post-doc-39	616.12	618.09	2.48	71.814	72.224 e63
49X-4, 19-20	PhD-13	616.19	618.16	2.59	71.822	72.232
49X-4, 93-94	PhD-12	616.93	618.90	2.44	71.900	72.310 e64
49X-4, 101-102	post-doc-40	617.02	618.99	2.45	71.908	72.318
49X-5, 11-12	post-doc-41	617.62	619.59	2.38	71.965	72.375
49X-5, 20-21	PhD-8	617.70	619.67	2.37	71.973	72.383
49X-5, 80-81	PhD-5	618.30	620.27	2.45	72.039	72.449 e65
49X-5, 105-106	post-doc-42	618.56	620.53	2.65	72.070	72.480
49X-5, 135-136	PhD-1	618.85	620.82	2.49	72.097	72.507 e66
49X-6, 10-11	post-doc-43	619.11	621.08	2.49	72.111	72.521
49X-CC, 20-21	post-doc-44	619.50	621.47	2.44	72.133	72.543

50X-1, 10-11	post-doc-45	621.11	623.08	2.42	72.233	72.643	e67
50X-1, 93-94	post-doc-46	621.94	623.91	2.47	72.295	72.705	e68
50X-2, 11-12	post-doc-47	622.62	624.59	2.55	72.338	72.748	
50X-2, 101-102	post-doc-48	623.53	625.50	2.52	72.399	72.809	e69
50X-3, 10-11	post-doc-49	624.11	626.08	2.59	72.458	72.868	
50X-3, 110-111	post-doc-50	625.11	627.08	2.71	72.556	72.966	e70
50X-4, 10-11.5	post-doc-51	625.62	627.59	2.62	72.604	73.014	e71
50X-4, 101-102	post-doc-52	626.52	628.49	2.57	72.687	73.097	
50X-5, 11-12	post-doc-53	627.12	629.09	2.63	72.728	73.138	e72
50X-5, 100-101	post-doc-54	628.01	629.98	2.59	72.789	73.199	
50X-6, 16-17	post-doc-55	628.67	630.64	2.62	72.877	73.287	e73
50X-6, 110-111	post-doc-56	629.61	631.58	2.48	72.982	73.392	e74
50X-7, 10.5-11.5	post-doc-57	630.12	632.09	2.58	73.051	73.461	e75
50X-CC, 28.5-30	post-doc-58	630.50	632.85	2.60	73.100	73.510	e76
51X-1, 11-12	post-doc-59	630.62	632.97	2.53	73.110	73.520	
51X-1, 101.5-102.5	post-doc-60	631.53	633.88	2.71	73.191	73.601	e77
51X-2, 10-11	post-doc-61	632.11	634.46	2.73	73.222	73.632	
51X-2, 80-81	post-doc-62	632.81	635.16	2.70	73.259	73.669	
51X-3, 10-11	post-doc-63	633.61	635.96	2.80	73.308	73.718	e78
51X-3, 121.5-122.5	post-doc-64	634.73	637.08	2.71	73.396	73.806	e79
51X-4, 11-12	post-doc-65	635.12	637.47	2.64	73.431	73.841	
51X-4, 101-102	post-doc-66	636.02	638.37	2.76	73.505	73.915	e80
51X-5, 9-10	post-doc-67	636.60	638.95	2.77	73.544	73.954	
51X-5, 84-85	post-doc-68	637.35	639.70	2.69	73.594	74.004	e81
51X-6, 35-36	post-doc-69	638.36	640.71	2.66	73.656	74.066	
51X-6, 130-131	post-doc-70	639.31	641.66	2.72	73.713	74.123	e82
52X-1, 10-11	post-doc-71	640.11	642.46	2.68	73.759	74.169	
52X-1, 65-67	post-doc-72	640.67	643.02	2.63	73.791	74.201	e83
52X-2, 4-5	post-doc-73	641.55	643.90	2.62	73.838	74.248	
52X-2, 112-113	post-doc-74	642.63	644.98	2.76	73.896	74.306	e84
52X-3, 10-12	post-doc-75	643.12	645.47	2.66	73.924	74.334	
52X-3, 77-78	post-doc-76	643.78	646.13	2.67	73.970	74.380	
52X-4, 10-11.5	post-doc-77	644.62	646.97	2.67	74.028	74.438	
52X-4, 109-110.5	post-doc-78	645.61	647.96	2.55	74.097	74.507	
52X-5, 10.5-11.5	post-doc-79	646.12	648.47	2.66	74.132	74.542	
52X-5, 98-99	post-doc-80	646.99	649.34	2.58	74.193	74.603	
52X-6, 8-9	post-doc-81	647.59	649.94	2.57	74.235	74.645	
52X-6, 83-85	post-doc-82	648.35	650.70	2.56	74.288	74.698	
52X-7, 11-12	post-doc-83	649.12	651.47	2.56	74.341	74.751	
52X-CC, 5-6	post-doc-84	649.38	651.73	2.58	74.360	74.770	
53X-1, 12-13	post-doc-85	649.63	652.25	2.64	74.396	74.806	
53X-1, 100-102	post-doc-86	650.52	653.14	2.67	74.458	74.868	
53X-2, 1-2	post-doc-87	651.02	653.64	2.57	74.492	74.902	
53X-2, 89-90	post-doc-88	651.90	654.52	2.65	74.554	74.964	
53X-3, 9-10	post-doc-89	652.60	655.22	2.52	74.602	75.012	
53X-3, 101-102	post-doc-90	653.52	656.14	2.54	74.666	75.076	
53X-4, 15-16	post-doc-91	654.16	656.78	2.65	74.711	75.121	
53X-4, 108-109	post-doc-92	655.09	657.71	2.58	74.776	75.186	
53X-5, 40-41	post-doc-93	655.91	658.53	2.51	74.833	75.243	
53X-5, 148-149	post-doc-94	656.99	659.61	2.62	74.908	75.318	
53X-6, 18-19	post-doc-95	657.19	659.81	2.51	74.922	75.332	
53X-6, 101-102	post-doc-96	658.02	660.64	2.66	74.979	75.389	
53X-7, 1-2	post-doc-97	658.52	661.14	2.88	75.014	75.424	
53X-CC, 14-15	post-doc-98	658.75	661.37	2.71	75.030	75.440	
54X-1, 76-77	post-doc-99	659.77	662.39	2.76	75.101	75.511	
54X-1, 138-139	post-doc-100	660.39	663.01	2.74	75.144	75.554	
54X-2, 58-59	post-doc-101	661.09	663.71	2.62	75.193	75.603	
54X-2, 121-122	post-doc-102	661.72	664.34	2.64	75.237	75.647	
54X-3, 15-16	post-doc-103	662.16	664.78	2.66	75.267	75.677	
54X-3, 111-112	post-doc-104	663.12	665.74	2.80	75.334	75.744	
54X-4, 46-47	post-doc-105	663.97	666.59	2.69	75.393	75.803	
54X-4, 120-121	post-doc-106	664.71	667.33	2.71	75.445	75.855	
54X-5, 95-96	post-doc-107	665.96	668.58	2.89	75.532	75.942	
54X-6, 60-62	post-doc-108	667.12	669.74	2.87	75.612	76.022	
54X-6, 128-129	post-doc-109	667.79	670.41	2.80	75.659	76.069	
54X-7, 20-21	post-doc-110	668.21	670.83	2.57	75.688	76.098	
54X-CC, 25-26	post-doc-111	668.50	671.91	2.69	75.763	76.173	
55X-1, 11-12	post-doc-112	668.62	672.03	2.84	75.772	76.182	
55X-1, 66-67	post-doc-113	669.17	672.58	2.84	75.810	76.220	

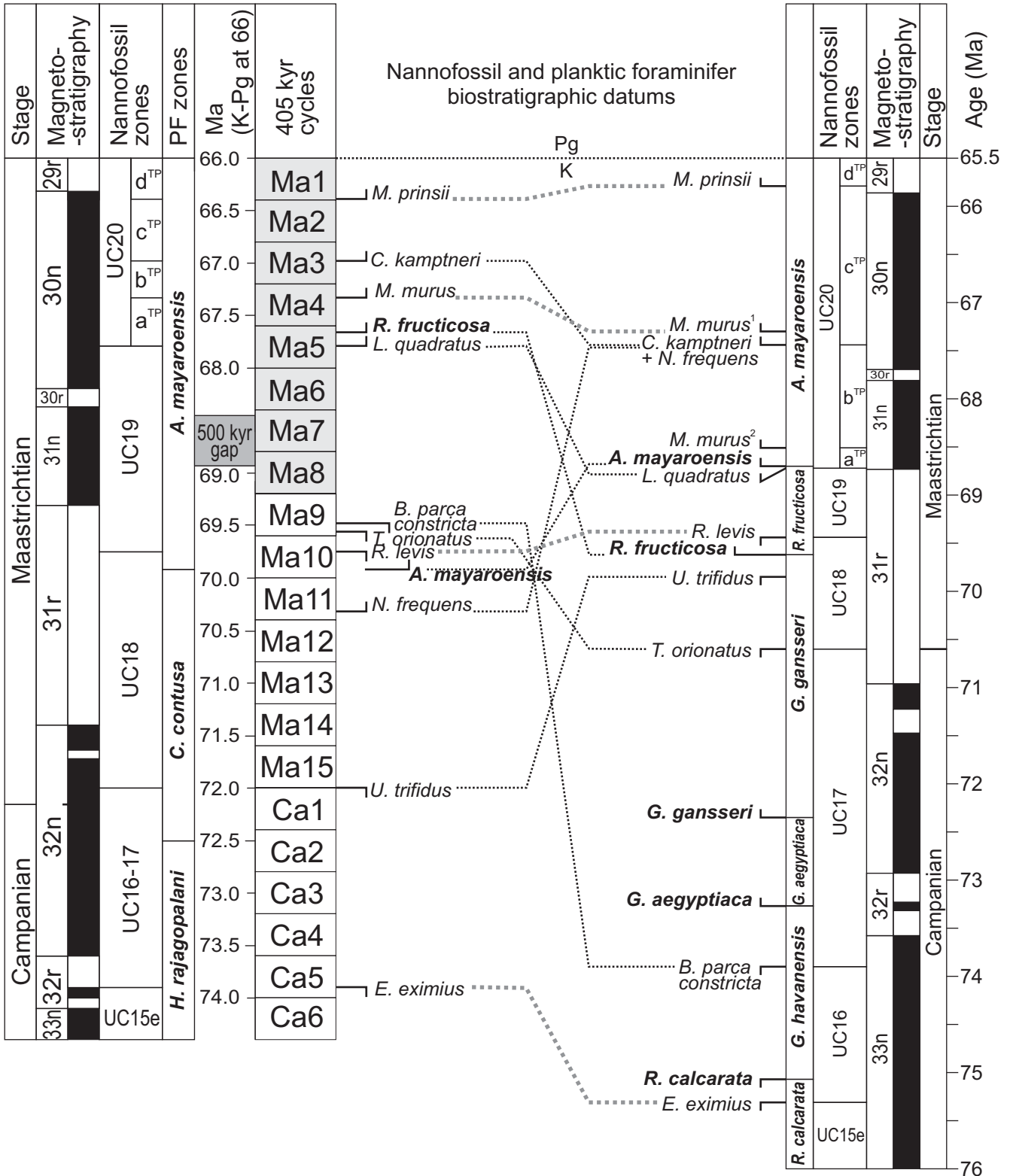
Based on an average sedimentation of 14.5 m/Ma



Appendix 6

Exmouth plateau
age model based
on Hole 762C

Conventional model
based on Gradstein et al. (2004)
and Huber et al. (2008)



Appendix 7